Critical Analyses and Fundamental Theoretical Developments in Computational Chemistry

Acronym: CRAFT

Scientific report for 2017-2019

I. Critical verification of the current used basis sets. Testing the limits of Density Functional Theory (DFT) methods.

I.A. Stating the problems existing with the currently used bases. Testing the spectral performances of the Gaussian bases for the hydrogen atom.

The computational chemistry[1] is a distinct branch of modern fundamental science and at the same time a valuable counterpart of the applied material sciences, providing explanations and predictions as guidelines for achieving desired properties. The vast majority of quantum chemical calculations is based on the so-called Gaussian Type Orbitals (GTOs)[2] which represent the "concrete and steel" of the actual development in this field. Alternative options such as the Slater Type Orbitals (STOs) are rarely used, in spite of the fact that these would represent rational conceptual choice. In solid state problems, but also applicable (in certain circumstances) at molecular level, the Plane Wave (PW) are often employed.

We will launch here a caveat about drastic problems and hidden limitations in the use of Gaussian basis sets. An important test of basis sets is given by the case of hydrogen atom, for which correct analytical solutions are known. Confined to the non-relativistic Schrödinger equation, the orbital eigenvectors are done by the Laguerre polynomials, which can be described as combinations of $r^k \cdot \exp(-Z \cdot r/n)$ components, with k running from 0 to n-1, for a given n main quantum number (Z being the general nuclear charge of the one-electron atom). The eigenvalues are, simply, $E_n = -Z/(2n^2)$, irrespective the $l = 0, \ldots n$-1 secondary quantum numbers subsequent to a given n index.

From this brief description one may foresee the engineering approach to the wavefunction problem of the hydrogen atom. Namely, even without knowing about Laguerre functions, just having a hint, a guess, that the $r^k \cdot \exp(-\zeta \cdot r)$ primitives are close to the aimed solutions, then such functions can be set as a basis for the matrix representation of the corresponding Hamiltonian. The r^k factors, with $k>0$, are playing essential role in determining the long-range shape of the radial atomic orbitals, namely the positions of nodes and extrema at relatively large n quantum numbers. It is well known that the widespread use of GTOs instead of STOs implies a compromise but is tacitly believed that the most affecting part is the use of $\exp(-\zeta \cdot r^2)$ exponentials instead of the $\exp(-\zeta \cdot r)$ ones. However, the hidden drawback is that, addressing a shell with the l quantum number, the GTOs are implying a unique r^l cofactor, instead of a r^k series, e.g. ranging from k=0 to k=n-l-1, if get inspiration from the expansion of Laguerre polynomials in STO primitives. Then, for instance the s-type GTOs consist only in linear combination of pure exponentials, without any r^k cofactor. This impinges upon the radial profiles and computed orbital energies. Since the problem at hand is specific, to avoid the use of the full engine of one the existing electronic structure code, we produced our own code for the GTO-based Hamiltonian representation of the hydrogen atom, outlined in the Table I.1. There is a large variety of used GTOs (e.g. Pople-type bases,[3] Ahlrichs sets,[4] correlation consistent cc-pv*n*z,[5] Atomic Natural Orbitals ANO bases,[6] Effective Core Potential ECP series,[7]), however most of them faulted even in the H case.

Table I.1. The Matlab-Octave code for the calculation of H atom with general GTO bases (taken from a input file).

```
function [leig,e,c]=readgto1(filename)
% e.g. filename='h-cc-pv5z.gto'
fid=fopen(filename,'r'); title1=fgetl(fid);
linegto=fgetl(fid);
endtest=length(findstr(linegto,'*'));
nfct=0;nprim=0; while endtest==0
nfct=nfct+1;
    aaa=sscanf(linegto,'%s %i %g ',3);
if char(aaa(1))=='S' | char(aaa(1))=='s'
    lshell=0;
elseif char(aaa(1))=='P' | char(aaa(1))=='p'
    lshell=1;
elseif char(aaa(1))=='D' | char(aaa(1))=='d'
    lshell=2;
elseif char(aaa(1))=='F' | char(aaa(1))=='f'
    lshell=3;
elseif char(aaa(1))=='G' | char(aaa(1))=='g'
    lshell=4;
elseif char(aaa(1))=='H' | char(aaa(1))=='h'
    lshell=5;
elseif char(aaa(1))=='I' | char(aaa(1))=='i'
    lshell=6;
elseif char(aaa(1))=='K' | char(aaa(1))=='k'
    lshell=7;
else
    lshell=-1;
end
    ngto=aaa(2);
lfct(nfct)=lshell;
for i=1:ngto
 ac=fscanf(fid,'%g %g ',2);
 aexp(i)=ac(1);
 cexp(i)=ac(2);
 nprim=nprim+1;
  bas(nprim,1)=lshell+1;
bas(nprim,2)=lshell; bas(nprim,3)=ac(1);
 cgto(nprim,nfct)=ac(2);
end
linegto=fgetl(fid);
endtest=length(findstr(linegto,'*'));
end
%eig(hmat,smat)
[c0,e0]=eig(hmat,smat);
snl=diag(power(diag(c0'*smat*c0),-1/2));
c1=c0*snl;
[e1,iord]=sort(diag(e0));
c2=c1(:,iord);

rmin=0;
rmax=10;
dr=0.05;
r=rmin:dr:rmax;

for k=1:length(r)
    for i=1:nprim
rbas(i,k)=rgto(bas(i,1),bas(i,3),r(k));
end:end
rbas1=cgto'*rbas;
end
```

```
ca=smat^(1/2)*c2;
leiga=diag(ca'*diag(lfct)*ca);
ea=e1;
[leiga,ea]
e=e';
[leig,e]
reig1=c3'*rbas1;
plot(r,reig1)
c=smat^(1/2)*c3;
leig=diag(c'*diag(lfct)*c);

reig=c2'*rbas1;
kont=0;
for i=1:nfct
sg=1;
  if max(abs(reig(i,:)))==max(-(reig(i,:)))
      sg=-1;
  end
c2(:,i)=sg*c2(:,i);
if e1(i)<=0
    kont=kont+1;
c3(:,kont)=c2(:,i);
e(kont)=e1(i);
end
%disp(bas)
Z=1;
ngto=inline('sqrt((2^(3/2+n)*a^(1/2+n))/ga
mma(1/2+n))','n','a');
rgto=inline('sqrt((2^(3/2+n)*a^(1/2+n))/ga
mma(1/2+n))*power(r,n-1)*exp(-
a.*r^2)','n','a','r');

for i=1:nprim
    for j=1:nprim
n1=bas(i,1);l1=bas(i,2);a1=bas(i,3);
n2=bas(j,1);l2=bas(j,2);a2=bas(j,3);
if l1==l2 ; l=l1;

s=(gamma((1/2)*(n1+n2+1))/(a1+a2)^((1/2)*(
n1+n2+1)))*sqrt(((2*a1)^(n1+1/2)*(2*a2)^(n
2+1/2))/(gamma(n1+1/2)*gamma(n2+1/2)));
h=((a2^2*(1+l^2+n1-n1^2)+a1*a2*(-
1+2*l+2*l^2+n1+n2+2*n1*n2)+a1^2*(l+l^2+n2-
n2^2))*gamma((1/2)*(-1+n1+n2))-
2*(a1+a2)^(3/2)*Z*gamma((n1+n2)/2))*    ...
(1/(2*(a1+a2)^((1/2)*(n1+n2+3))))*sqrt(((2
*a1)^(n1+1/2)*(2*a2)^(n2+1/2))/(gamma(n1+1
/2)*gamma(n2+1/2)));

else
h=0;s=0;
end
hmat0(i,j)=h;
smat0(i,j)=s;
end
end
hmat=cgto'*hmat0*cgto;
smat=cgto'*smat0*cgto;
```

The Table I.A1 from appendix shows the results obtained from the assessment of an extended, almost exhaustive, series of current basis sets. A rigorous treatment would give only negative energies, $-1/(2n^2)$. The positive values represent leftovers of the applied technique. All the existing basis sets are approximating reasonably or well the -0.5 a.u. energy for 1s. The vast majority fails in giving negative energy even for 2s level. The highly rated cc-pV*n*Z (n=D,T,Q, 5, 6) bases give negative energy for 2s, but with bad absolute value. An isolated surprise is the Sadlej+ basis, accounting the sign and approximate values up to n=6. This prompts for the future aimed reconsideration of the bases and computing codes.

I.B. Verifying the performances of existing bases and the DFT limits for the d and f metal ions. Correlations with Slater-Condon parameters.

Plane Wave methods as source for radial profiles of atomic orbitals. After starting with the simplest atom, the hydrogen, we go now for heavier elements, testing the other extreme of periodic table. Thus, we devoted our attention to methodological issues related to the study of electronic structure of lanthanide ions and complexes, particularly using plane-wave-based methods. Despite the apparent simplicity, the atomic calculations of lanthanides show several aspects under debate.[8,9] Specifically, will consider atoms with the $6s^25d^14f^n$ electronic configuration. Within the considered projected-augmented wave (PAW) computational method, with VASP code,[10] the configuration of lanthanide atoms is $[Xe]5s^25p^26s^25d^14f^n$, namely with the electrons of [Xe] core replaced by the effective potentials.

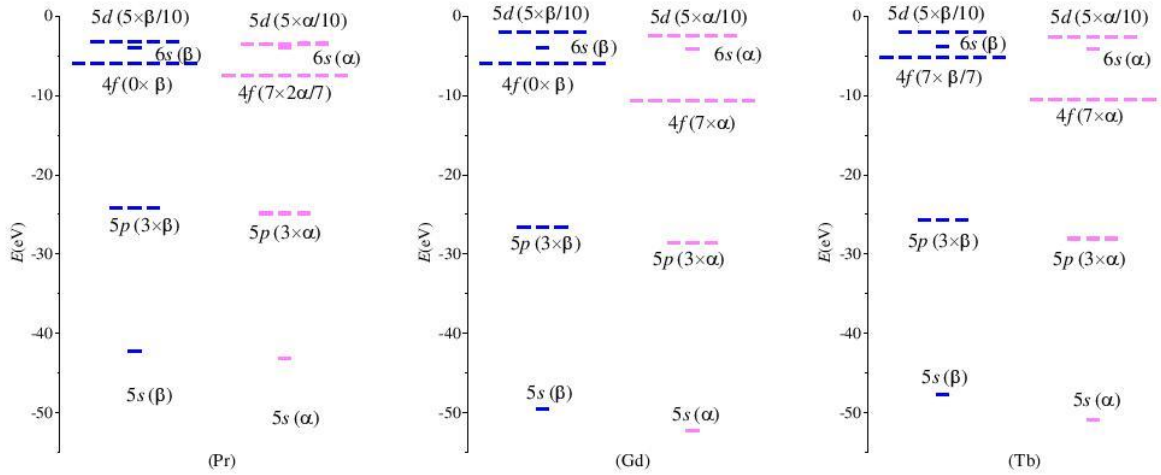

Figure I.1. Orbital levels of selected lanthanide atoms, Pr, Gd and Tb, computed by DFT (PBE functional) within Gamma-zero option, with VASP code, under specific control of non-*aufbau* configuration.

We will consider the spin polarization only for the f shell, while the electrons in 4s and 5d are paired in their shells. In order to keep the spherical nature of the atom, fractional occupations are considered for the incomplete degenerate orbital sets. Namely, for the f^n shell, each atomic orbital (AO) should have a $n/7$ occupation. For the elements in the first half of the lanthanide series ($n<7$) there are $n/7$ α electrons and empty β subsystem. For instance, the Pr(III) ion has the f^2 configuration, corresponding to 2/7~ 0.285714 population of each f α-type AO. At the middle of the series, the Gd(III) has an integer occupation of AOs, with $n=7$ and the half-filled $f^{7\alpha}$ shell. After the middle of the series, the $f^{7\alpha}$ configuration is kept, the fractional occupation going into the β part. For instance, the Tb(III) ion, with the $f^8=f^{7\alpha}f^{1\beta}$ configuration has 1/7~0.142857 electrons in each β-type f orbital. In all cases, the outer 5d shell is considered using fractional occupations, spinless, with 0.5α+0.5β configuration, e.g. the d^1 electron being smeared as 0.5α and 0.5β fractional occupations of each component of the unrestricted d-type shell.

In the figure I.1 we selected several cases, such as the Pr, Gd and Tb atoms. Practically, all the systems are non-*aufbau*, since the upper 5s and 4d orbitals are occupied, above the partly filled or empty f shell components. For the Pr atom, this occurs in both α and β subsystems (considering the partly filled $f^{2\alpha}$ and the empty $f^{0\beta}$). At half-occupation (i.e. Gd), or after it (Tb-Yb), the non-*aufbau* configuration occurs for the β electrons. We managed the non-*aufbau* calculations with the help of occupation keywords (FERWE and FERDO in VASP). We

checked that the non-*aufbau* sequences, e.g. {1,3,0,1,0.5} for the β-{5s,5p,4f,6s,5d} on Pr(III) or Gd(III) are lower in energy than the *aufbau* series reordering {5s,5p, 6s,5d 4f}, avoiding pushing the empty β-f shell above the occupied AOs. Since in the lanthanide systems the basic optical and magnetic properties, also interesting for application purposes, are due to atomic-like features it is worth focusing on the detailed study of the f atomic orbitals.

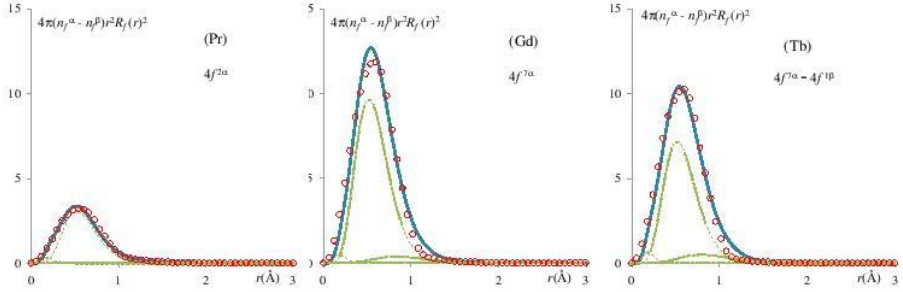

Figure I.2. Radial profile of the spin difference density, accounting for 2 electrons in the Pr example, 7 electrons for Gd and 6 electrons for the Tb case (proportional to the area under curves). The results from VASP atomic calculation are shown by circles and the continuous line corresponding to the fit with a combination of three Slater-Type Orbitals (STOs), represented by dashed lines.

An interesting result, extracted from the above calculation, is the radial profile of the spherical section in the volume occupied by the f electrons (see Figure I.2). It is obtained from the maps of α minus β electron densities, representative completely for the f shell. The radial profile from plane-wave calculations allows us to fit the 4f node-less AO as combination of Slater-type orbitals (STOs) and, from here, to estimate the Slater-Condon two-electron parameters, which will provide the Coulomb (U) and exchange (J) parameters to be employed in a DFT+U scheme. Thus, with the following functions:

$$R_{STO}(n,\zeta,r) = N_{STO}(n,\zeta)\cdot r^{n-1}\exp(-\zeta\cdot r), \qquad N_{STO}(n,\zeta) = \sqrt{\frac{(2\zeta)^{2n+1}}{(2n)!}} \tag{I.1}$$

the atomic orbitals are obtained as linear combinations of STOs:

$$R_{AO}(r) = \sum_{i=1}^{N} a_i R_{STO}(n,\zeta,r) \tag{I.2}$$

Taking for the 4f shell three components with n=4, for the selected atoms, the resulted parameters are presented in Table I.2.

Table I.2. Parameters of the f atomic shell subsequently obtained to the plane –wave calculation of selected lanthanide atoms. The coefficients (a_i) and exponents (ζ_i) of the three STO primitives fitting the radial pattern and the resulted Slater-Condon electron-electron parameters (F_k).

	Pr	Gd	Tb
a_1	0.16784	0.10800	0.13298
a_2	0.84917	0.80185	0.74674
a_3	0.20868	0.19800	0.24380
ζ_1	11.396	11.514	11.464
ζ_2	4.043	4.080	4.065
ζ_3	1.465	2.546	2.642
F_0(cm^{-1})	170997.17	171793.78	170254.73
F_2(cm^{-1})	368.15	393.86	383.14
F_4(cm^{-1})	48.35	52.79	51.04
F_6(cm^{-1})	5.18	5.70	5.50

The 4f shell treated by a $r^3\exp(-\zeta r)$ single exponential leads to the following analytic Slater-Condon parameters:

$$F_0 = \frac{26333}{131072}\zeta \;,\quad F_2 = \frac{459}{917504}\zeta \;,\quad F_4 = \frac{697}{10092544}\zeta \;,\quad F_6 = \frac{697}{5622988}\zeta \qquad \text{(I.3)}$$

The relative ratio of the parameters, in the order of increasing subscript is 26580.8: 66.2:9.1:1. For multi-exponential AOs, the expressions are becoming more complex, but yet tractable. Then, with the fitted radial parameters, the Slater-Condon quantities can be obtained. The calculated values are reasonably close to the experimental ones, particularly considering that the traditional Gaussian-based methods are leading to systematic overestimations of the F_k parameters. The spectral experiments do not enable the F_0 parameter (which determines a common shift of all the spectral terms). For the F_2, F_4, F_6 series on Pr(III) the experiment yield the 316.7, 58.7, 5.5 respective values, all in cm^{-1}.[11] This compares well with the estimated 368.15, 48.35, 5.18 amounts (in cm^{-1}). As mentioned, the gaussian based multiconfiguration methods are overestimating the leading F_2 parameter, having for instance, for Pr(III), the 439.9, 56.5, 6.0 (cm^{-1}) values with the effective core-type SBKJC basis and 431.8, 55.7, 5.9 (cm^{-1}) with the all-electrons SARC basis.

Non-standard calculations for Ligand-Field and exchange interactions by CAS and DFT methods d-f systems.

In the following we will assess properties tuned by the basis set quality, namely the Ligand Field (LF) and exchange coupled parameters.[12] We considered the problem of d-f exchange coupling in the binuclear Cu-Gd system,[13] treated by Broken Symmetry (BS)[14,15] approach. For a Cu-Gd complex the BS method consists in two unrestricted calculations with S_z(HS) =7/2+1/2=4 and S_z(BS)=7/2-1/2=3 projections for the so-called High Spin (HS) and Broken Symmetry states (BS). The calculations were done with GAMESS code[16] using the SBKJC effective core potentials and basis sets for Gd while 6-311G* for the Cu and 6-31G for the C or H atoms. The molecular structure is taken for the experimental Cu-Tb system,[17] assuming the same skeleton for the Cu-Gd. The Density Functional Theory (DFT) calculations[18] were performed, mainly with B3LYP functional.

We consider two calculations whose spin populations on the Cu and Gd sites reflect the spin switching, the exchange coupling constant is obtained by extracting the energy, E, and spin square expectation value, $\langle S^2 \rangle$ from unrestricted DFT calculations, using the Yamaguchi-Onishi formula[19]:

$$J = \frac{E_{BS} - E_{HS}}{\langle S^2 \rangle_{HS} - \langle S^2 \rangle_{BS}} \qquad \text{(I.4)}$$

The exchange parameter estimated with B3LYP functional, J_{CuGd}=+1.85 cm^{-1} is in agreement to the experimental one,[13] J_{CuGd}=+2.1 cm^{-1} (in the formalism ascribing the exchange Hamiltonian as $\hat{H} = -2J\ \hat{S}_1 \cdot \hat{S}_2$). The Mulliken spin populations from Table I.2 show that the computation is in agreement with the idea of BS treatment, having values close to the {Gd(7α),Cu(α)} vs. {Gd(7α),Cu(β)} configurations for HS vs BS states. This situation is also well illustrated in Figure I.3 plotting the spin density. One observes that the density maps are similar in absolute contour, but that the BS has opposite spin around the Cu atom. A part of the spin density in the d-type coordination sphere is delocalized over the surrounding atoms. The density on the f centre is almost perfectly spherical, compatible with the symmetry of the half-filled shell.

Table I.3. Details of the BS-DFT calculations on the Cu-Gd system with B3LYP functional

State	Energy (atomic units)	$\langle S^2 \rangle$	Mulliken Spin Populations	
			Gd	Cu
HS{Gd(7α),Cu(α)}	-4440.30370943	20.013	7.030	+0.727
BS:{Gd(7α),Cu(β)}	-4440.30365016	13.013	7.028	-0.725

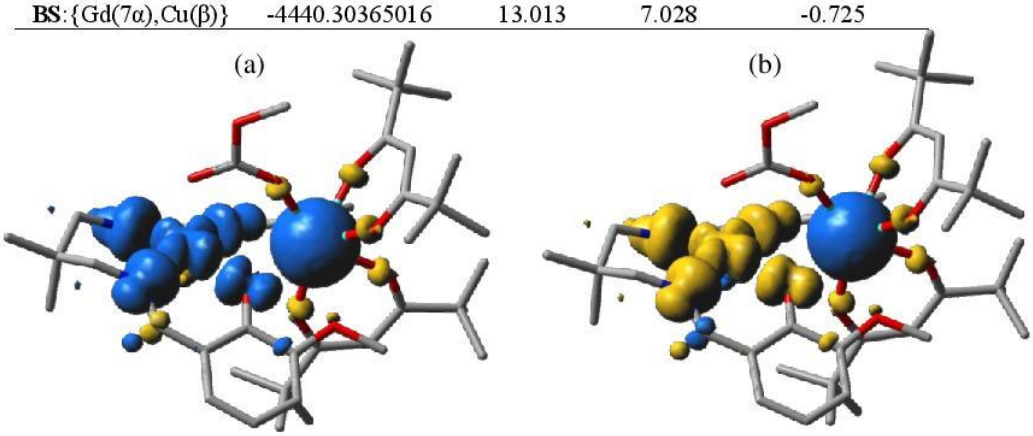

Figure I.3. Spin density maps for the B3LYP calculations on the Cu-Gd complex: (a) the HS case, (b) the BS case. The surface is drawn at 0.001e/Å^3, with α spin density in blue and β spin density in yellow.

In order to confirm the relationship of the obtained results against the basis set factors, we embraced the plane-waves paradigm, where is possible to mimic the case of infinite basis. Here we used the VASP code, sampling the *k*-space with only Gamma point, considering that the molecular aspects are in focus, not the band structure pattern.

If the cluster is placed in a box of size 30 Å, a first-set of calculations performed failed to converge. The box size appears to be too large and the computational cost is prohibitive. Therefore, we decided to reduce the box size to 20 Å, and once properly checked, the convergence, we re-run the calculations in a larger cell (a 25 Å–size cubic cell) in order to evaluate size-effects. Potentials used (POTCAR) are PBE type. For Gd-potential semicore s- and p-states are included as valence states: Gd potential has 18 valence electron in the electronic configuration ($5s^2p^6$)($4f^7$)($6s^2$ $5d^1$), and Cu potential has 11 valence electrons, in the configuration ($3d^{10}$) ($4s^1$). To treat the electronic correlation for Gd and Cu atoms, as standard procedure in DFT, we used GGA+U approach in the Dudarev formalism.[20] Specifically, we included the following values for Hubbard-like correlation parameter U: $U_{gd\text{-}f}$=6 eV, $U_{cu\text{-}d}$=6 eV. The energy cutoff for the plane-wave basis set was fixed to 400 eV, and the Gamma point was considered for the integration in the Brillouin zone.

The calculations are performed first for the paramagnetic (non-spin polarized) state of the binuclear CuGd-cluster, then the converged charge density and wavefunctions used to achieve convergence of the two spin-polarized magnetic states (HS and BS), with proper initialization of atomic magnetic moments for Gd and Cu atoms, and constrained the total magnetic moments to the expected values, namely 8 μ_B for HS state and 6 μ_B for BS state. Unfortunately, the plane-wave environment does not provide expectation value of the spin square operator, confining then to an Ising-type formula in the analysis of BS results:

$$J = \frac{E_{BS} - E_{HS}}{4S_1S_2} \quad . \qquad \text{(I.5)}$$

In our case the denominator equals 4×(1/2) ×(7/2)=7. Taking, comparatively, the denominator from previous Yamaguchi-type formula one observes that is exactly 7, ensuring us that Ising type estimation is valid too. The above described calculations yields then a *J*=2.65

cm-1 coupling constant, relatively close to the Gaussian-type DFT calculation and to experimental values. We then evaluated the effect of size of the simulation cell on the Cu-Gd magnetic exchange coupling, by performing the same set of calculations for a cluster in a box of size 25 Å (see Table I.4a)

Table I.4a. The tuning of the molecular box in PW-BS-DFT calculations.

Box-size (Å)	20	25
$\Delta E_{BS\text{-}HS}$ (meV)	2.30	2.29
J (cm^{-1})	2.65	2.64

We find a small reduction of the magnetic exchange (~0.4%) by increasing the box-size. This seems a negligible difference and we continue to work with the 20 Å-box model. We then evaluate the convergence of the $\Delta E_{BS\text{-}HS}$ with respect to energy cutoff of the plane-wave basis set used. We checked for three cut-off values: 350, 400 and 450 eV (Table I.4b).

Table I.4b. The effect of tuning the tuning the cut-off parameter in PW-BS-DFT calculations.

En-Cutoff (eV)	350	400	450
$\Delta E_{BS\text{-}HS}$ (meV)	2.32	2.30	2.30
J (cm^{-1})	2.67	2.65	2.65

The convergence is achieved for the cut-off value used for all the calculations (400 eV). This value can be taken as basis-set free evaluation of the exchange coupling. We now evaluate the effect of U-correlation parameter on the magnetic exchange and calculate $\Delta E_{BS\text{-}HS}$ (meV) - $_{HS}$ for the cases: GGA (no-correlation included), $U_{Cu\text{-}d}$, $U_{Gd\text{-}f}$, and compare with the previous calculation ($U_{Cu\text{-}d}$ and $U_{Gd\text{-}f}$), as seen in Table I.4c.

Table I.4c. The effect of tuning the tuning the Coulomb-Correlation parameter in DFT+U calculations.

U-correlation	GGA	$U_{Cu\text{-}d}$=6eV	$U_{Gd\text{-}f}$=6eV	$U_{Cu\text{-}d}$ =$U_{Cu\text{-}d}$=6eV
$\Delta E_{BS\text{-}HS}$ (meV)	0.74	1.23	3.29	2.30
J (cm^{-1})	0.85	1.42	3.79	2.65

Here the total magnetic moments are unchanged for the HS and BS magnetic states, 8 and 6 μ_B respectively. The magnetic ground state is given by ferromagnetic coupling for Cu-Gd for all U-cases considered, and we notice that inclusion of correlation of Cu- and Gd-sites has counteracting effects: while increased correlation of Gd-site clearly favors ferromagnetism (ΔE goes from 0.74 to 3.29 meV), the inclusion of U on Cu-site favors the AF-exchange pathway (ΔE reduces to 2.30 meV).

We will explore in the following the limits of the DFT approach, attempting to produce different components originating from the Ligand Field (LF)[21] splitting of the ^7F multiplet, using the leverage of initial orbital permutation. Namely, taking the natural orbitals generated by the Cu-Gd calculations (i.e. post-computationally handled functions having occupations restricted pattern, with occupation number close to 1), we prepare the initialization of the input in several way, running the orbital where the β electron of the f^8 configuration of Tb(III) will be placed. In this manner, we investigate the possibility to mimic the multiplet nature, if the states with different starting orbitals converge to different solutions. The fact that we obtain different configurations in the different SCF processes is illustrated as in figure I.4, taking the difference density maps with respect of the Cu-Gd reference. We take this global manner of characterization since the f-type β electron is smeared among several MOs and there is no simple orbital way of graphical characterisation.

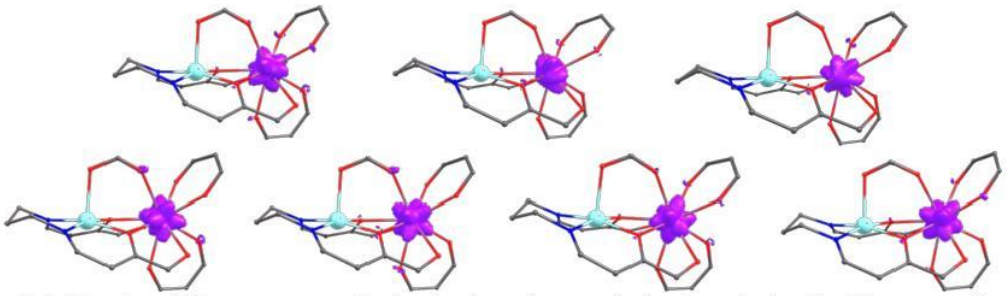

Figure I.4. Density difference maps obtained subtracting total density of the Cu-Gd system from the corresponding series of different orbital configurations of the Cu-Tb congener. The shape of the surfaces (contours with six or eight lobes) suggest the accommodation in f-type MOs for the β electron, when compare the f^8 and f^7 systems.

Table I.5. DFT emulation of the the levels associated with the Ligand Field split and the ^7F term of the Tb(III) site, by initiating DFT calculation with permuted MOs. Comparatively, CAS data are shown.

	DFT				CAS		
	ΔE_{HS} (cm^{-1})	ΔE_{BS} (cm^{-1})	J (cm^{-1})		ΔE_{HS} (cm^{-1})	ΔE_{BS} (cm^{-1})	J (cm^{-1})
1	0.0	9.5	1.59		0.0	5.3	0.76
2	170.6	180.4	1.62		11.7	16.7	0.72
3	228.5	238.2	1.61		211.0	216.1	0.73
4	259.4	270.4	1.84		272.5	277.5	0.72
5	363.1	373.3	1.70		597.7	602.6	0.70
6	1517.9	1531.1	2.21		626.3	632.2	0.85
7	2363.9	2375.1	1.87		813.8	819.6	0.83

For each of the seven configurations taken as surrogates the F term levels, we considered the HS and BS calculation tuned by the spin polarization of the copper centre. The energies of the configurations (see Table I.5) in a given spin state (HS or BS) series, are a measure of LF splitting of the f shell on the Tb site. The gap between HS and BS energies at a fixed configuration yields the exchange coupling constant. It is interesting to see that the magnitude of the coupling results almost the same on all the seven LF-type states. The LF total or successive gaps are over-estimated in comparison to the expected range (a total split of several hundreds of cm^{-1} units). Probably the cause is the fact that, in unrestricted frame, separation of α and β orbital energies is not in line with the LF modelling paradigm. In turn, the CAS (Complete Active Space) methods are retrieving well the LF range.

II. Reconstructing the basis sets. New bases, at conceptual and technical levels.

II.A. Conceiving and writing the algorithms for the treatment of many-electrons atom in the wave-function and density functional theories. (Obj. D.2.1.1 and D.2.1.2)

To approach the audacious aims of the project, must conceive our own codes, since the envisaged improvements are beyond the offer of the existing programs for atoms and molecules. In order to reach the full generality in the frame of wave-function theory, the procedure must be equivalent with state-averaged complete active spaces (CAS) with arbitrary occupations of atomic shells. In the case of the atom, the state averaging ensures objects with spherical symmetry. The procedure can be converted in Fock-alike self-consistent field (SCF) orbital optimization admitting general occupations, p_{l_i}, over the whole set of shells, l denoting the quantum number and i counting the repetition of the given shell type:

$$E = \sum_l \sum_i p_{l_i} h_{l_i} + \sum_l \sum_i \left\{ \frac{1}{2} p_{l_i} (p_{l_i} - 1) F^0_{l_i l_i} + e_x[p_{l_i}, p, \sigma_{l_i}, J_{l_i l_i}] \right\} +$$

$$\sum_{l \le l'} \sum_{l_i \ne l'_{i'}} \left\{ p_{l_i} p_{l'_{i'}} \left(F^0_{l_i l'_{i'}} - \frac{1}{2} J_{l_i l'_{i'}} \right) - 2\sigma_{l_i} \sigma_{l'_{i'}} \cdot J_{l_i l'_{i'}} \right\} \quad . \qquad \text{(II.1)}$$

The h_{l_i} elements are the orbital one-electron energies (kinetic and electron-nuclear parts), the $F^0_{l_i l_i}$ and $F^0_{l_i l'_{i'}}$ are the respective intra- and inter-shell Coulomb integrals, while the $J_{l_i l_i}$ and $J_{l_i l'_{i'}}$ are the corresponding averaged exchange integrals. For a l^n sub-configuration, having $n \equiv p_{l_i}$ electrons in the l_i shell, more exactly with n_α spin-up and n_β spin-down particles, the $\sigma_{l_i} = (n_\alpha - n_\beta)/2$ denotes the net spin of the shell. The shell-distributed spin quantities are summed to the total spin of the atom $S = \sum_l \sum_i \sigma_{l_i}$.

A key ingredient in the atomic total energy is the exchange inside a given shell denoted by e_x in the previous expression. By induction on a series of particular cases, we arrived at the following equation:

$$e_x[l, p, \sigma, J_{ll}] = -\frac{2l+1}{2l+2} J_{ll} \sigma(\sigma + 1) - p \cdot \left(\frac{1}{4}(p - 2) + \frac{p - 4l - 2}{8(l+1)} \right) J_{ll} \quad . \qquad \text{(II.2)}$$

In the particular class of situations, but yet a sufficiently large frame, when all the partial spins on the shells have the same polarization, the exchange part turns into:

$$e_x[l, p, \sigma, J_{ll}] = -\frac{p}{8(l+1)} [(2l + 3)p - 2(4l + 3)] J_{ll} - \frac{2l+1}{2l+2} \sigma \cdot (\sigma + 1) J_{ll} \quad . \qquad \text{(II.3)}$$

The J_{ll} are the average values of the exchange integrals over all the orbital couples within a given shell. For the respective s, p, d and f cases, these quantities are:

$$J_{ss} = 0 \quad , \qquad \text{(II.4.a)}$$

$$J_{pp} = \frac{1}{5} F^2_{pp} = 5F^{pp}_2 \quad , \qquad \text{(II.4.b)}$$

$$J_{dd} = \frac{1}{14} F^2_{dd} + \frac{1}{14} F^4_{dd} = \frac{7}{2} \left(F^{dd}_2 + 9F^{dd}_4 \right) \quad , \qquad \text{(II.4.c)}$$

$$J_{ff} = \frac{2}{45} F^2_{ff} + \frac{1}{33} F^4_{ff} + \frac{50}{1287} F^6_{ff} = 10F^{ff}_2 + 33F^{ff}_4 + 286F^{ff}_6 \quad , \qquad \text{(II.4.d)}$$

as function of Slater-Condon radial parameters. [22] There are two conventions for Slater-Condon parameters, with the k rank indices annotated as superscripts or subscripts, mutually converted by specific factors. In the case of the above intra-shell parameters the F^k_{ll} vs. F^{ll}_k relationships are understood from the outlined (II.4.a)-(II.4.c) formulas. The Table II.1 shows the formulas for the inter-shell exchange integrals. The diagonal contains the same type of shells, but different functions.

Table II.1. Generic formulas for inter-shell averaged exchange integrals.

	s	p	d	f
s	$J_{s_1s_2} = G^0_{n_1sn_2}$			
p	$J_{ps} = J_{sp} = \frac{1}{3}G^1_{sp}$	$J_{p_1p_2} = \frac{1}{3}G^0_{n_1pn_2p} + \frac{2}{15}G^2_{n_1pn_2p}$		
d	$J_{ds} = J_{sd} = \frac{1}{5}G^2_{sd}$	$J_{dp} = J_{pd} = \frac{2}{15}G^1_{dp} + \frac{3}{35}G^3_{dp}$	$J_{d_1d_2} = \frac{1}{5}G^0_{n_1dn_2d} + \frac{2}{35}G^2_{n_1dn_2d} + \frac{2}{35}G^4_{n_1dn_2d}$	
f	$J_{fs} = J_{sf} = \frac{1}{7}G^3_{sf}$	$J_{fp} = J_{pf} = \frac{3}{35}G^2_{fp} + \frac{4}{63}G^4_{fp}$	$J_{fd} = J_{df} = \frac{3}{35}G^1_{fd} + \frac{4}{105}G^3_{fd} + \frac{10}{231}G^5_{fd}$	$J_{f_1f_2} = \frac{1}{5}G^0_{n_1fn_2f} + \frac{2}{35}G^2_{n_1fn_2f} + \frac{2}{77}G^4_{n_1fn_2f} + \frac{100}{3003}G^6_{n_1fn_2f}$

The Coulomb and exchange integrals are decomposed in four-orbital two-electron integrals over the primitive elements of the given basis. We realized an extensive work, programming the corresponding formulas for both Slater-type Orbitals (STO) and Gaussian-type Orbitals (GTO). A general two-electron integral (either in STO or GTO bases) is:

$$R^k(n_al_a, n_bl_b, n_cl_c, n_dl_d) = \int_{r_1=0}^{\infty}\int_{r_2=0}^{\infty} R_{n_al_a}(r_1)R_{n_cl_c}(r_1)R_{n_bl_b}(r_2)R_{n_dl_d}(r_2)\frac{min(r_1,r_2)^k}{max(r_1,r_2)^{k+1}}r_1^2r_2^2dr_1dr_2\,. \quad \text{(II.5)}$$

The $G^k_{n_al_a,n_bl_b}$ type integrals (see Table II.1) result from the above formula in the $n_al_a = n_cl_c$ and $n_bl_b = n_dl_d$ case. In the $n_al_a = n_cl_c = n_bl_b = n_dl_d$ situation, one achieve the $F^k_{n_al_a,n_al_a}$ integrals. The F^k and G^k -type integrals for the eigenvectors are expanded in the general R^k integrals over the basis primitives.

To the best of our knowledge, a closed formula for the atomic energy of atomic body, as function of general shell occupation numbers, is not presented in the specialized literature, particularly in the concern of the intra-shell exchange terms fulfilling the meaning of state-averaged CAS. The above considerations are valid for the wave-function theory (WFT) approach of the atomic bodies.

In order to switch to the density functional theory (DFT) must adapt the exchange terms with elements representing the exchange-correlation functionals:

$$E = \sum_l \sum_i p_{l_i} h_{l_i} + \frac{1}{2}\sum_{l,l'}\sum_{l_i \neq l'_{i'}}\left\{p_{l_i}\left(p_{l'_{i'}} - \delta(l_i, l'_{i'})\right)F^0_{l_il_i} + p_{l_i}p_{l'_{i'}}\cdot J_{l_il'_{i'}}\right\} \quad \text{(II.6.a)}$$

where

$$J_{n_il_i,n_jl_j} = \int_{r=0}^{\infty} R_{n_il_i}(r)R_{n_jl_j}(r)V_{xc}\left(\rho_\alpha(r), \rho_\beta(r)\right)r^2dr, \quad \text{(II.6.b)}$$

while ρ_α and ρ_β are the spin-up and spin-down densities. We confined ourselves to the simplest functional, Local Density Approximation (LDA). While in the WFT version all the integrals are done analytically, the J terms in the DFT version are integrated by numeric quadrature.

II.B. Optimizing new Gaussian-type basis sets for the series of first light atoms. (Obj. D.2.1.2)

As pointed previously, the nowadays quantum chemical is heavily based based on the so-called Gaussian Type Orbitals (GTOs).[23,24] The radial form of an atomic GTO primitive, as function of radius r (i.e. the departure of the electron from the nucleus), depends on the parameter inside the exponential (ζ) and a certain factor as a power of radius, r^{k-1}, ascribed as:

$$R_{\mathrm{GTO}}(k,\zeta,r) = \left(\frac{2(2\zeta)^{\frac{2k+1}{2}}}{\Gamma\left(\frac{2k+1}{2}\right)}\right)^{1/2} \cdot r^{k-1} \cdot \exp(-\zeta \cdot r^2) \quad , \qquad \text{(II.7)}$$

where Γ is the incomplete Gamma function.[25] There is a rich variety of GTOs, all undergoing a hidden drawback. The problem with the GTOs does not stay only in the $\exp(-\zeta r^2)$ part, as the quasi-totality of users (and even developers) seem to believe, but in a wrong design of the polynomial cofactors. Namely, for all the Gaussian basis sets in use the k factor in the above formula is strictly limited to the l+1 value with respect to the l quantum number specific to a shell (l=0, 1, 2 … for respective s, p, d etc). In the previous stage we discussed in detail this aspect for the hydrogen atom. Now will advance toward the first elements of the periodic table. We propose a well-proportionated scheme taking m elements of $r^{k-1}\cdot\exp(-\zeta r^2)$ form for each k subset belonging to a l shell, with k in the l+1:n range, confining the n value to the maximal level for which the good description of the spectrum is desired.

Table II.2. The fit of the GTO $R_{\mathrm{GTO}}(k,\zeta,r)$ functions for second row of the periodic table. The first column contains the definition of pre-exponential factors, the content of the table consisting in the ζ exponential parameters (in Bohr^{-2}).

	k	Li	Be	B	C	N	O	F	Ne
s	1	0.00221	0.01371	0.00401	0.07071	0.00540	0.00629	0.00727	0.00991
	1	0.24895	1.07233	0.58312	3.94029	0.87066	1.07033	1.29241	1.66180
	1	28.10699	83.85794	84.71342	219.57834	140.28768	182.13684	229.78998	278.75371
	2	0.00287	0.00534	0.00865	0.02728	0.00634	0.00735	0.00833	0.00907
	2	0.14176	0.33489	0.43243	1.27506	0.47877	0.58858	0.70496	0.81221
	2	7.00890	21.00679	21.60758	59.60180	36.14519	47.13183	59.65897	72.72299
	3	0.00353	0.00220	0.00503	0.00891	0.00733	0.00852	0.00961	0.01008
	3	0.08887	0.12259	0.18738	0.44144	0.29270	0.36066	0.43139	0.48842
	3	2.23826	6.81691	6.98521	21.88176	11.68365	15.27249	19.36171	23.67305
p	2	0.00764	0.01525	0.01749	0.00941	0.00780	0.00859	0.02872	0.02639
	2	0.05404	0.32359	0.44032	1.06329	0.29523	0.34774	0.78835	0.84922
	2	0.38239	6.86518	11.08270	120.17749	11.17023	14.08015	21.63916	27.33244
	3	0.00921	0.00843	0.00836	0.01140	0.00549	0.00604	0.00560	0.00766
	3	0.06526	0.14110	0.18189	0.42871	0.13807	0.16239	0.21428	0.26619
	3	0.46268	2.36271	3.95736	16.12051	3.47500	4.36262	8.19443	9.24446
	4	0.00352	0.00371	0.00390	0.00518	0.00611	0.00673	0.00656	0.00956
	4	0.04357	0.06433	0.08315	0.16886	0.09101	0.10611	0.15800	0.19305
	4	0.53982	1.11514	1.77409	5.50665	1.35551	1.67188	3.80271	3.89907
d	3	0.00872	0.00897	0.00909	0.00903	0.00894	0.00888	0.00883	0.00880
	3	0.02464	0.02586	0.02646	0.02614	0.02573	0.02540	0.02517	0.02501
	3	0.06964	0.07454	0.07701	0.07569	0.07400	0.07267	0.07174	0.07109

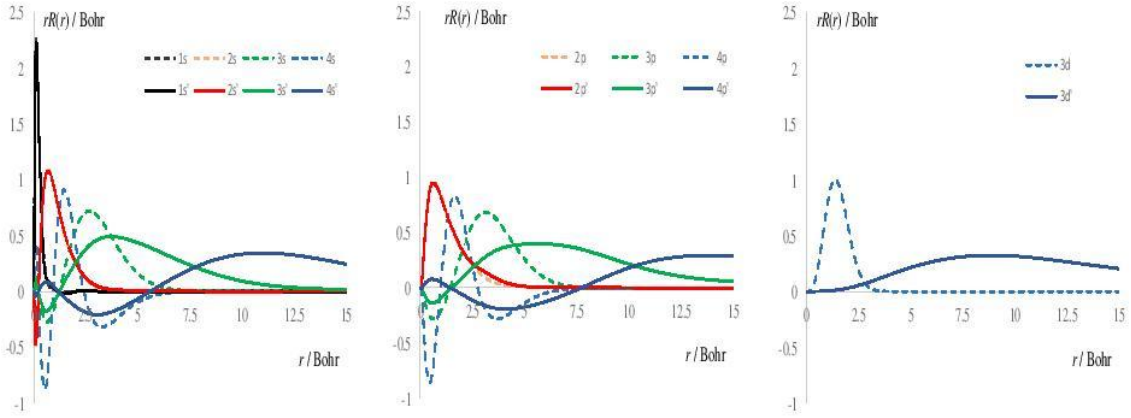

Figure II.1. The $r \cdot R(r)$ profiles for the Ne atom, with GTOs, in the LDA method. Dashed lines: the results from the 6-31+G* standard basis. Continuous lines: new basis (see Table II.2).

We chose to optimize the exponents of the Li-Ne series in the DFT frame, taking the LDA functional and restricted spinless scheme. For the s-type orbitals we convened to use three primitives with k=1, three ones with k=2 and three with k=3, targeting the fit of the 1s-4s orbitals (i.e. two virtuals). For the p shell we considered three primitives for k=2, three for k=3, and also three elements for k=4, fitting the 2p-4p shells. The 3d shell was treated by three GTOs with k=3. The results are presented in the Table II.2. The Figure II.1 compares the new basis with a consecrated one, 6-31+G*, taking the Ne atom. One observes that, while the occupied atomic orbitals (1s,2s,2p), are similar in both treatments, the new basis enables radially more expanded virtuals, as proven correct in the previous stage of the project.

II.C. Optimizing new Slater-type basis sets for the series of first light atoms. (Obj. D.2.1.3) Relationships with numeric basis sets. (Obj. D.2.1.5)

Alternative option for atomic basis sets are represented by the Slater Type Orbitals (STOs) [26],

$$R_{\mathrm{STO}}(k,\zeta,r) = \left(\frac{(2\zeta)^{2k+1}}{(2k)!}\right)^{1/2} \cdot r^{k-1} \cdot \exp(-\zeta \cdot r)\,, \qquad \text{(II.8)}$$

These are rarely used, [27] although these would represent a rational choice, suggested by the known exact solution for the hydrogen atom. Using a similar pattern of the radial factors similar to the above discussed GTO sets, we optimized the STOs for the same series of light atoms. The fit was realized to numeric orbitals produced by solving the DFT mean-field as a differential equation, following a methodology due to C. Daul, inspired from the making of effective potentials for plane-wave codes.[28] The numeric points are established by an exponential template, denser at origin and sparse at large distances:

$$r_k = \delta r_0 \frac{exp(kh)-1}{exp(h)-1}\,, \qquad \text{(II.9)}$$

where h is an asymmetry parameter and δr_0 is the first gap, from the r=0 point. The maximal number of points placed below a $r_{\max}$ radial limit is:

$$n_{max} = int[\frac{1}{h} ln\left(1 + r_{max}\frac{exp(h)-1}{\delta r_0}\right)]\,, \qquad \text{(II.10)}$$

where the square brackets containing the right-side member denote the integer of the comprised value. The differential equations are formulated as an eigenvalue problem, with the $P_k = r_k R(r_k)$ amplitudes as radial functions on the r_k poles. As function of Coulomb (C) and exchange-correlation (xc) potentials, the equations are organized as a tri-diagonal matrix:

$$\left(\frac{-1}{(r_{k+1}-r_{k-1})(r_k-r_{k-1})}, \frac{1}{(r_{k+1}-r_k)(r_k-r_{k-1})} - \frac{Z}{r_k} + \frac{1}{2}\frac{l(l+1)}{r_k^2} + V_C[\rho(r_k)] + V_{xc}[\rho(r_k)], \frac{-1}{(r_{k+1}-r_{k-1})(r_{k+1}-r_k)}\right) \cdot (P_{k-1}, P_k, P_{k+1})^T = E_l P_k \,. \quad \text{(II.11)}$$

The non-diagonal elements perform the numeric estimation of the second derivative implied by the kinetic energy. The resulted numeric $R(r)$ profiles were fitted with STO primitives, optimizing the mixing coefficients and the ζ exponents. The results are presented in Table II.3.

Table II.3. The fit of the STO $R_{\mathrm{STO}}(k,\zeta,r)$ functions for second row of the periodic table. The first column contains the definition of pre-exponential factors, the content of the table consisting in the ζ exponential parameters (in Bohr^{-1}).

	k	Li	Be	B	C	N	O	F	Ne
s	1	0.09247	0.01757	0.18381	0.00142	0.04903	0.17461	0.17903	0.18328
	1	0.57217	0.19232	0.95161	0.17892	1.21377	1.57709	1.77752	1.97487
	1	3.54033	2.10483	4.92668	22.47745	30.04607	14.24447	17.64808	21.27933
	2	0.04092	0.02020	0.02943	0.01445	0.00398	0.00698	0.00645	0.00608
	2	0.32886	0.20219	0.92925	0.44556	0.24988	0.27554	0.29034	0.30544
	2	2.64295	2.02414	29.34064	13.73827	15.69802	10.87256	13.06884	15.34886
	3	0.08605	0.02430	0.05428	0.00834	0.00965	0.01471	0.01376	0.01304
	3	0.39638	0.24507	0.52379	0.26595	0.30001	0.34438	0.36179	0.37880
	3	1.82589	2.47149	5.05437	8.48351	9.33021	8.06016	9.51219	11.00226
p	2	0.02142	0.01604	0.01122	0.21174	0.00196	0.01791	0.03108	0.36664
	2	0.11627	0.14593	0.88038	1.04239	1.30552	1.72735	0.36959	1.52949
	2	0.63100	1.32742	69.05852	5.13163	870.45106	166.59155	4.39468	6.38044
	3	0.02690	0.01803	0.02421	0.01224	0.02483	0.02513	0.03059	0.06472
	3	0.54397	0.77470	0.40438	0.25999	0.48322	0.51546	0.29616	0.56845
	3	10.99940	33.29156	6.75468	5.52122	9.40591	10.57383	2.86759	4.99317
	4	0.03241	0.02094	0.01882	0.02247	0.01700	0.03209	0.06219	0.02485
	4	0.37985	0.45269	0.25752	0.28780	0.29133	0.30098	0.32482	0.31508
	4	4.45152	9.78589	3.52388	3.68651	4.99172	2.82333	1.69656	3.99531
d	3	0.03053	0.07363	0.07000	0.06248	0.05580	0.05024	0.04577	0.04192
	3	0.33337	0.33450	0.33503	0.33476	0.33439	0.33409	0.33388	0.33372
	3	3.64033	1.51967	1.60354	1.79366	2.00372	2.22181	2.43564	2.65663

II.D. Realizing correlations between basis sets and the Slater-Condon parameters. (Obj. D.2.1.4)

The radial parts of the atomic orbitals are directly determining the so-called Slater-Condon parameters, which, in their turn, are establishing the spectroscopy of the atomic species. We devised codes for the computation and adjustment of the Slater-Condon parameters as function of a given basis sets. We will treat the atoms of several representative non-metal elements.

In the case of carbon atom, the lowest levels are due to the $(2s)^2(2p)^2$ valence configuration. Avoiding the explicit account of $(2s)^2$ part, one may deal directly with the two

electrons in the triply degenerate *p* shell. There are three types of spectral terms emerging from the p^2 configuration, ^{1}S, ^{1}D and ^{3}P, with the following energies:

$$E\left[\,^3P\right] = F_0^{2p,2p} - 5F_2^{2p,2p} \qquad \text{(II.12.a)}$$

$$E\left[\,^1D\right] = F_0^{2p,2p} + F_2^{2p,2p} \qquad \text{(II.12.b)}$$

$$\mathrm{E}[^1\mathrm{S}] = \mathrm{E}_{\mathrm{M_L}=0}\text{-}3\mathrm{E}[^1\mathrm{P}]\text{-}5\mathrm{E}[^1\mathrm{D}] = \mathrm{F}_0^{2\mathrm{p},2\mathrm{p}} + 10\mathrm{F}_2^{2\mathrm{p},2\mathrm{p}} E\left[\,^1S\right] = F_0^{2p,2p} + 10F_2^{2p,2p}$$

(II.12.c)

Considering that the Slater-Condon parameters are positive, one may easily see that ^{3}P is the ground term. The experimental split by spin-orbit is small, with the *J*=0, 1 and 2 states at the relative 0, 16.4 and 43.4 cm^{-1}(NIST).[29] Subtracting the barycentre of the spin-orbit multiplet, the other states ^{1}D and ^{1}S appear at 10163 cm^{-1} and 21618 cm^{-1}. Taking the formal gaps to these states with respect of ^{3}P groundstate as $.6F_2^{2p,2p}$ and $15F_2^{2p,2p}$, respectively, one may find two estimations of the $\mathrm{F}_2^{2\mathrm{p},2\mathrm{p}} F_2^{2p,2p}$: 1693 cm^{-1} and 1441 cm^{-1}. Taking the barycentre of the excited states (weighted with their multiplicity) one finds the average estimate $F_2^{2p,2p}$ =1609.62 cm^{-1}. Considering the eigenvector obtained with the LDA treatment and the above optimized STO primitives, one obtains $F_2^{2p,2p}$ =1911.10 cm^{-1}, i.e. a slight overestimation. The parameter can be brought exactly to the experimental average, performing a rotation between the canonical 2p and 3p orbitals with the {0.98534, 0.17057} vector.

Arriving at the nitrogen atom, one finds the situation of half-filled p shell, in the $(2s)^2(2p)^3$ configuration. The terms resulting from this configuration are ^{4}S (groundstate resulted from applying the *aufbau* principle, with all electrons parallel), ^{2}P and ^{2}D, having the following energies:

$$\mathrm{E}[^4\mathrm{S}] = \mathrm{E'}_{\mathrm{core}} + 3\mathrm{f'}_{2\mathrm{p}} + 3\mathrm{F}_0^{2\mathrm{p},2\mathrm{p}}\text{-}15\mathrm{F}_2^{2\mathrm{p},2\mathrm{p}} E\left[\,^4S\right] = 3F_0^{2p,2p} - 15F_2^{2p,2p},$$

$$\text{(II.13.a)}\mathrm{E}[^2\mathrm{D}] = \mathrm{E'}_{\mathrm{core}} + 3\mathrm{f'}_{2\mathrm{p}} + 3\mathrm{F}_0^{2\mathrm{p},2\mathrm{p}}\text{-}6\mathrm{F}_2^{2\mathrm{p},2\mathrm{p}}$$

$$E\left[\,^2D\right] = 3F_0^{2p,2p} - 6F_2^{2p,2p}, \qquad \text{(II.13.b)}$$

$$E\left[\,^2P\right] = 3F_0^{2p,2p} \quad . \qquad \text{(II.13.c)}$$

Relative to the ^{4}S groundstate, the ^{2}D and ^{2}P energies are about 19228 cm^{-1} and 28839 cm^{-1}, respectively. Taking their barycentre and equalling it with $(45/4)F_0^{2p,2p}$, one obtains the 2029.52 cm^{-1} for the 2p-2p Slater-Condon parameter. The canonical 2p orbital from the above STO fit yields the 2355.15 cm^{-1} overestimated value, the adjustment being realized with the {0.98680, 0.16193} mix of the primary 2p and 3p forms.

The case of the oxygen is, algebraically, similar to the carbon atom, since the p^4 configuration can be regarded as two holes placed in a filled p^6 shell, paralleling then the p^2 situation, the formal energies being:

$$E\left[\,^3P\right] = 6F_0^{2p,2p} - 15F_2^{2p,2p} \qquad \text{(II.14.a)}$$

$$E\left[\,^1D\right] = 6F_0^{2p,2p} - 9F_2^{2p,2p} \qquad \text{(II.14.b)}$$

$$\mathrm{E}[^1\mathrm{S}] = \mathrm{E}_{\mathrm{M_L}=0}\text{-}3\mathrm{E}[^1\mathrm{P}]\text{-}5\mathrm{E}[^1\mathrm{D}] = \mathrm{F}_0^{2\mathrm{p},2\mathrm{p}} + 10\mathrm{F}_2^{2\mathrm{p},2\mathrm{p}} E\left[\,^1S\right] = 6F_0^{2p,2p}$$

(II.14.c)

The wavenumbers of the excited states, ^{1}D and ^{1}S terms, are placed at 15815 cm^{-1} and 33740 cm^{-1}, respectively. The different terms may give two estimations of the $F_2^{2p,2p}$ intra-shell parameter, respectively 2636 cm^{-1} and 2249 cm^{-1}, or 2507 cm^{-1} from the barycentre. The direct STO estimation yields 2790.31 cm^{-1}, adjusted to the exact value with the price of the {0.99097, 0.13409} vector transformation between the nominal 2p and 3p, yielding therefore an approximation to the correlated 2p basis.

II.E. Adjusting basis sets for the d and f elements by optimization to experimental atomic spectra and Slater-Condon parameters. (Obj. D.2.1.4)

We will take as example for the treatment of the d-type transition elements the case of the Ni(II) free ion. The experimental data of Ni(II) ion (NIST) show a rather visible spin-orbit split of the ground term, ^3F_J, with relative values 0, 1360.7 cm^{-1}and 2269.6 cm^{-1} for respective J=4, 3 and 2 sub-multiplets. The barycentre of this set estimated as the average with the 2J+1 weights, is 993.9 cm^{-1}. Extracting this amount from the energies of other terms (these averaged too, when spin-orbit multiplets appear), the levels are $E(^1D)$= 13037.6 cm^{-1}, $E(^3P)$= 15836.3 cm^{-1}, $E(^1G)$= 22114.7 cm^{-1} and $E(^1S)$= 51538.0 cm^{-1}. For d elements is convenient to convert the Slater-Condon integrals in the so-called Racah parameters:

$A = F_0^{dd} - 49F_4^{dd}$, $B = F_2^{dd} - 5F_4^{dd}$ and $C = 35F_4^{dd}$ (II.15.a-c)

The analytic expressions of spectral terms, as function of Racah parameters, from table encapsulated in the Figure II.2 can be fitted, by least square procedures, obtaining the B=1154.5 cm^{-1} and C=3946.6 cm^{-1} values, rendering the following numeric approximations: $E_{fit}(^1D)$= 13665.8 cm^{-1}, $E_{fit}(^3P)$= 17317.5 cm^{-1}, $E_{fit}(^1G)$= 21747.3 cm^{-1} and $E_{fit}(^1S)$= 53025.5 cm^{-1}.

L\S	*S*=0	*S*=1
S	28*A*-28*B*+28*C*	0
P	0	28*A*-35*B*+21*C*
D	28*A*-45*B*+23*C*	0
F	0	28*A*-50*B*+21*C*
G	28*A*-38*B*+23*C*	0

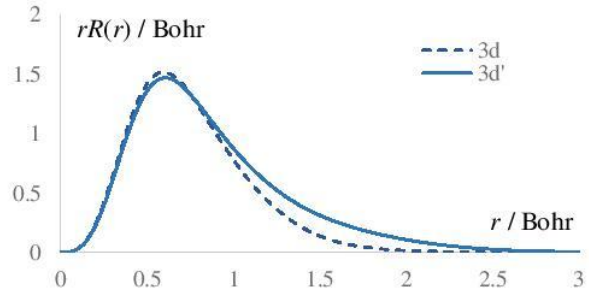

Figure II.2. Synopsis of the Ni(II) treatment, illustrative for the d-type elements. Left side: table of analytic formulas for the spectral terms, as function of Racah parameters. Right side: the $r{\cdot}R(r)$ radial profile of the canonical 3d orbital (dashed line) compared with those adjusted to the retrieval of experimental Racah parameters.

The calculation done with optimized STO primitives (prepared with a numeric LDA treatment) yields the B=1214.82 cm^{-1} and C=4450.47 cm^{-1} values. This can be adjusted by a remix between 3d and 4d functions, with the {0.99275, 0.12017} coupling, retrieving the B=1092.58 cm^{-1} and C=3962.27 cm^{-1} values, close to the experimental set. From the right side of the Figure II.2, one observes that the adjusted parameters are obtained with a profile slightly more extended at larger radii (labelled 3d'), as compared with the canonical 3d function.

The lanthanide series will be exemplified by the case of the Nd(III) free ion, performing procedures similar to those exposed at the above d-metal ion discussion. First, will consider the experiment data, obtained from the handling of optical multiplets. All the spin quartet terms and a part of the doublets have simple linear formulas as function of the Slater-Condon parameters (See left side of the Figure II.3). There are several data available: ^4F, ^4G and ^2K, relative to the ^4I groundstate, at the 10207 cm^{-1}, 16040 cm^{-1} and 17210 cm^{-1} barycentres, respectively. These are sufficient for an estimate the experimental parameters: F_2^{ff} = 362.79 cm^{-1}, F_4^{ff} = 44.81 cm^{-1} and F_6^{ff} = 6.86 cm^{-1}.

$$E[^4I] = 0$$
$$E[^4F] = 35F_2^{ff} + 42F_4^{ff} - 637F_6^{ff}$$
$$E[^4S] = 35F_2^{ff} + 42F_4^{ff} - 637F_6^{ff}$$
$$E[^4G] = 55F_2^{ff} + 66F_4^{ff} - 1001F_6^{ff}$$
$$E[^4D] = 90F_2^{ff} + 108F_4^{ff} - 1638F_6^{ff}$$
$$E[^2K] = 25F_2^{ff} + 142F_4^{ff} + 259F_6^{ff}$$
$$E[^2P] = 40F_2^{ff} + 97F_4^{ff} + 364F_6^{ff}$$

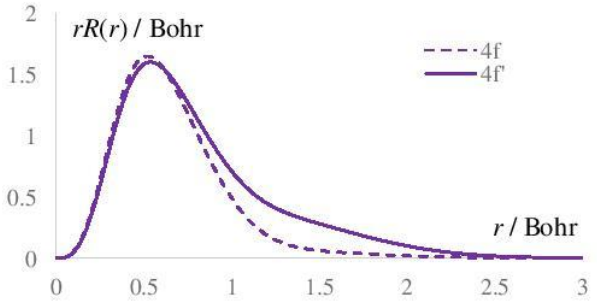

Figure II.3. Synopsis of the Nd(III) treatment, illustrative for the d-type elements. Left side: Analytic formulas for the spectral terms, as function of Slater-Condon parameters. Right side: the $r{\cdot}R(r)$ radial profile of the canonical 4f orbital (dashed line) compared with those adjusted to the retrieval of experimental F_{ff}^k parameters.

We optimized a basis having three STO primitives with k=4 preexponential factors and the ζ={0.138, 1.067, 8.277} set of exponents, aside two primitives with k=5 and ζ ={0.006, 4.415}. The canonical 4f orbitals lead to a certain over-estimation of the Slater-Condon parameters, as in all the above previously mentioned instances: F_2^{ff} = 466.85 cm^{-1}, F_4^{ff} = 60.40 cm^{-1} and F_6^{ff} = 6.42 cm^{-1}. Proceeding, as previously, to the coupled rotation of the 4f and 5f orbitals, one achieves a new 4f' shell with F_k^{ff} values closer the experimental data, 362.81 cm^{-1}, 46.36 cm^{-1} and 4.91 cm^{-1}, for the outlined parameters. The right side of the Figure II.3 shows that these results imply a certain "breathing" of the shell, reaching slightly expanded radial shape. The canonical orbitals have somewhat compressed radial profiles, as consequence of a compensation effect: the shrunk shape enforces larger positive energy of inter-electron repeal, while increases the modulus of negative energy of electron-nuclear attraction. The fit to experimental parameters of the electronic spectra prepares contracted bases with a better account of the correlation effects.[30]

II.F. Correlations between computed and experimental structural data. (molecular geometry, spectra, magnetism).

The application part concerns the magnetism of a new series of cyanide-bridged assemblies, {KH[Ln$_2$(2,3-pzdc)$_2$(CH$_3$OH)(H$_2$O)$_7$][M(CN)$_8$]}·5H$_2$O (Ln^{3+} = Nd, Gd, Tb, Dy; M^{4+} = Mo, W).[31] The setting *ab initio* calculations for lanthanide complexes is a non-trivial task, the delicate situation being a reliable orbital guess, to initiate the calculations. Therefore, a customized choice is a starting set which is produced by merging the fragment orbitals obtained in preamble for the free lanthanide ion and the remainder of the molecule. This setting describes most appropriately the weakly interacting f shell of the lanthanide ions. We retrieved the orbital components of the Zeeman Hamiltonian by extracting extra-output from the black box of the computation, namely the matrix elements of the L_x, L_y and L_z operators. This part, as well as the spin-type Zeeman, enabled the explicit implementation of the magnetic field dependence of the Hamiltonian and the *ab initio* simulation of the magnetic and optic properties of the considered systems. As seen in the right side of the Figure II.4, the first-principles simulation of the magnetic susceptibility leads to curves very close to the experimental ones, a remarkable fact, given the intrinsic complexity of the magneto-structural correlations in f-type complexes. The left side of the Figure II.4 illustrates the simulation of the full spectra from the f-type multiplets (in the upper part), with details of the lowest levels (in the bottom part). The split of the lowest multiplet is in principle visible as detail in the optical spectra. Although the actual measurements had not the sufficient resolution, the credit guaranteed in the general retrieval of magnetic properties, enables the computation as good predictive tool, replacing the

experimental missing information. Thus, one may predict (as the series of data shown in the left-bottom side of Figure II.4 shows) a strong dependence of the fine structure of the spectrum on the coordination sphere of the lanthanide ions. The considered systems are belonging to the class of Metal-Organic-Frameworks (MOFs), having a relatively strong 3D lattice and also some labile ligands (which can be partly eliminated or added, subsequently). The sensitivity of the spectral and magnetic properties to this geometry change allows the speculation on their functionality as sensors to small molecules, accommodated in the voids of the MOF lattice.

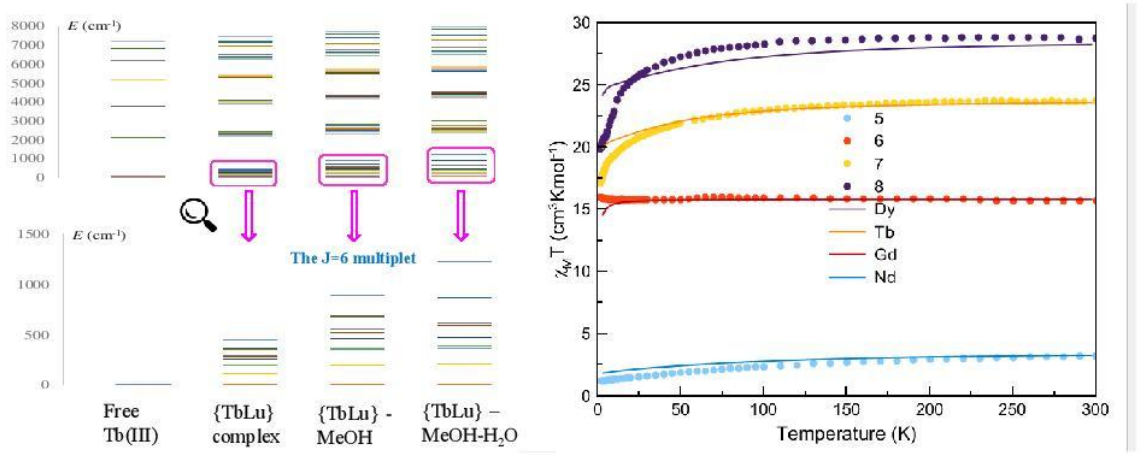

Figure II.4. Left panel: computed spectral multiplets of the complexes at different coordination geometries, after eliminating weakly bonded water and methanol ligands, considering for simplicity, that site 1 is occupied by spectrally inactive Lu, while site 2 has the Tb ion. Right side panel: Temperature dependence T vs. $\chi_M T$ of $\{KH[Ln_2(2,3\text{-pzdc})_2(CH_3OH)(H_2O)_7][W(CN)_8]\}\cdot 5H_2O$,(Ln=Nd, Gd, Tb,Dy) compounds. The continuous lines are marking the *ab initio* simulated curves.

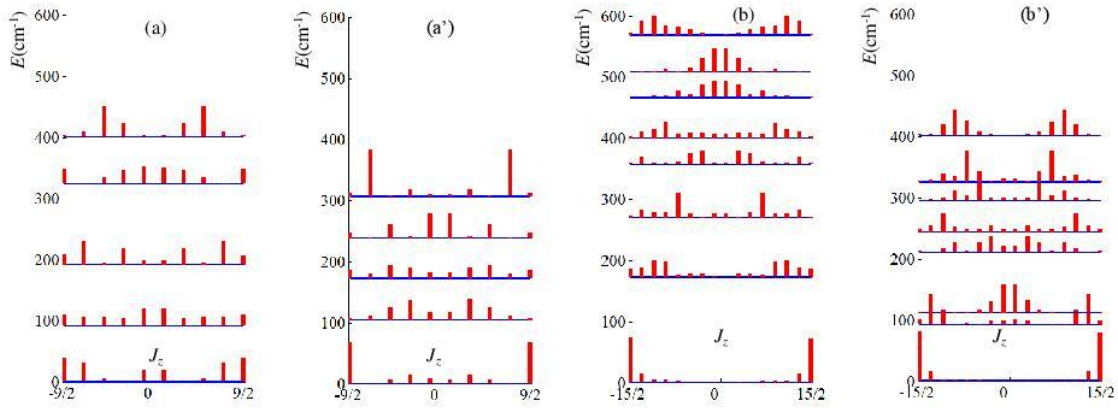

Figure II.5. The Ligand Field spectrum of the J ground multiplet of the Ln(III) ions in isomorphous complexes (left half, a and a'- Nd; right side, b and b' -Dy). The a and b panels correspond to site 1, while b and b' stand for site 2. The vertical bars at each levels mark, the percentage of J_z projections contributing to the given state

Aside the Slater-Condon parameters, discussed previously, the properties of the lanthanide ions in molecules or lattices are determined by the spin orbit (SO) coupling and

Ligand Field (LF) parameters, due to the immediate environment. Although, with special care the DFT treatments can be applied to lanthanide compounds, the proper approach belongs to wave function theories, namely via CAS methods. In a further insight, we revealed the composition of each state from the LF-determined *J* spectrum, in terms of J_z projections (See Figure II.5). The histograms drawn at each level corresponds to the relative percentage of the J_z elements in the corresponding wavefunction. The diagrams are symmetric with respect of the $\pm J_z$ couples. One observes that the groundstates are made preponderantly of elements close to the extremal projections, $J_z = \pm J$. Such a situation is well evidenced for the Dy case, where, for both sites, the groundstate consists in almost pure ±15/2 components. Comparatively, the Nd system has a spin admixed groundstate with comparable participation of the ±9/2 and ±7/2 terms, and a certain tail of ±1/2 elements. This suggests that, in the case of Nd(III), the f shell is more perturbed by the environment, while in the Dy(III), the lanthanide contraction leads to a somewhat more retracted radial profile (as our considerations on bases shows) and a more atomic-like character of ion in the molecule.

III. New functionals and functionalities in electronic density based-methods

III.A&B. The elaboration of the theory of a new type of density functional, respecting the spherical symmetry of the atom. (Obj. D.2.2.1). The relationship with the Slater-Condon parameters / The elaboration of the atoms' treatment codes with the new forms of the density functional in Gaussian, Slater or numerical basis sets for extended series of atoms. (Obj. D.2.2.2)

To reach the title objectives, one must prepare adequate ancillary tools in order to describe the exchange energy. In this view, we will proceed to the dichotomization of two-electron terms in components, doing their evaluation on numeric grids. Note that we are able and we do the full analytic calculation of two-electron integrals, repeating the procedure in the numeric mode only for detective purposes. The numeric integration over functions with exponential profiles is better done with a grid with exponential spacing of the points. Such an integration scheme, due to Weber *et al.*[32], uses the following definition for the *m*-th point:

$$r_m = \delta r_0 \frac{exp(mh)-1}{exp(h)-1} \ , \qquad \text{(III.1)}$$

depending on the spacing of the first point with respect of the origin, δr_0, and a scale parameter, *h*. Practically, the same grid is used in several other programs doing numeric calculations of the atoms with the purpose of preparing pseudo-potentials for plane-wave calculation, as is the case of ATOMPAW module from the ABINIT suite.

Deciding a maximal radial extension, the set, r_{max}, the number of points results as:

$$m_{max} = \left[\frac{1}{h} ln\left(1 + r_{max}\frac{exp(h)-1}{\delta r_0}\right)\right] \ , \qquad \text{(III.2)}$$

the square brackets meaning the integer taken from the function. Conversely, if desire a certain number of points over a given radial interval, must fit correspondingly the *h* parameter. The points are associated with a set of weights:

$$w_m = h \cdot \delta r_0 \frac{exp(mh)}{exp(h)-1} \ , \qquad \text{(III.3)}$$

so that the numeric integration of a given function $f(r)$ can be formulated as a weighted sum of the function over the grid:

$$\int_{r=0}^{\infty} f(r)dr \approx \sum_{m=1}^{m_{max}} w_m \cdot f(r_m) \ , \qquad \text{(III.4)}$$

a double sum of this sort being performed for two-dimensional integration.

Then, aiming for the account of a given exchange element, J_{ab}, the entities to be integrated over the 2D grid are:

$$X_{mn}^{ab} = r_m^2 r_n^2 R_a(r_m) R_b(r_m) R_a(r_n) R_b(r_n) \ \sum_{m=1}^{m_{max}} \chi_{ab}^k \cdot \frac{min(r_m,r_n)^k}{max(r_m,r_n)^{k+1}} \qquad \text{(III.5)}$$

The $\chi_{ab}{}^k$ coefficients are formalizing the definition of J_{ab} integrals for a given shell couple, ab, as combination of Slater-Condon parameters with k superscript. Conventionally, the m and n indices are running on the electrons labelled 1 and 2. One may produce a partial summation, emulating the integration over the electron #2, which corresponds the one-electron operator in the mean field treatment of an exchange element:

$$Y_m^{ab} \approx \sum_{n=1}^{n_{max}} X_{mn}^{ab} w_n \ \rightarrow \ \widehat{J_{ab}}(r_1) \qquad . \qquad \text{(III.6)}$$

The quantities produced from this partial integration will be used in the further analysis. The numeric estimation of the whole exchange coupling integrals can be termed as:

$$J_{ab} \approx \sum_{m=1}^{m_{max}} w_m \cdot \ Y_m^{ab} \ = \sum_{n=1}^{n_{max}} \sum_{m=1}^{m_{max}} w_m \cdot w_n \cdot X_{mn}^{ab} \qquad \text{(III.7)}$$

We probed that, in the calculations described below, the numerically estimated integrals are resembling in a fourth digit, or better (in atomic units), the analytic ones, working over a 300 points grid, established with the following parameters: δr_0=0.001 Bohr, r_{max}=20 Bohr and h=0.02.

With the leverage described at equation (III.6), one may select from the sum of total energy, in (4), the exchange components integrated only on one electron:

$$V_x^{ll'}(r_1) = \sum_{l \le l'} \sum_{l_i \ne l'_{i'}} \left\{ -p_{l_i} p_{l'_{i'}} \left(\frac{1}{2} + 2\sigma_{l_i} \sigma_{l'_{i'}} \right) \cdot \widehat{J}_{l_i l'_{i'}}(r_1) \right\} \ , \qquad \text{(III.8)}$$

$$V_x^l(r_1) = \sum_{l_i} [\alpha_l \cdot p_{l_i} + \beta_l \cdot p_{l_i}^2 + \gamma_l \cdot \sigma_{l_i}(\sigma_{l_i} + 1)] \widehat{J}_{l_i l_i}(r_1) \ , \qquad \text{(III.9)}$$

Then, summing over all the intra- and inter-shell contributions, we obtained the energy profiles of total exchange density, V_x.

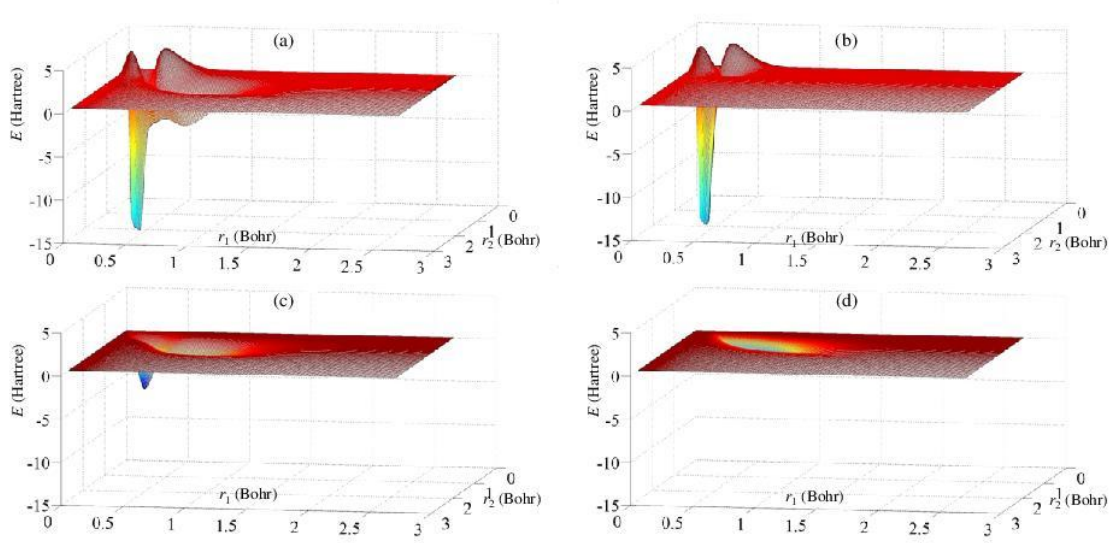

Figure III.1. The exchange energy distribution for Ne atom, as function of radial coordinates of formal electrons 1 and 2. (a) the total exchange energy; (b) the exchange due to inter-shell s-s interaction; (c) the s-p exchange coupling; (d) the exchange energy inside the p shell.

The Figure III.1 details the exchange energy in the X_{mn} components derived from equation (11) for the case of neon atom. The maps for the other atoms are looking qualitatively similar. The panel (a) sums all the contributions, at each point of the 2D radial grid. The other panels are detailing the distinct shell contributions. The panel (b) shows the interactions between the two *s* shells, which can be ascribed as $X_{mn}^{1s,2s}$. This shows positive zones, due to the negative 1s(r_1)2s(r_2) areas, whose action is amended with the negative sign of the exchange in the total energy, $-2J_{1s,2s}$. However, the total balance of the exchange is negative, due to net positiveness of the exchange parameters. The panel (c) shows the *s-p* inter-shell exchange, each point containing the $X_{mn}^{1s,2p} + X_{mn}^{2s,2p}$. The panel (d) shows the *p* intra-shell exchange, small in relative value, as compared to the other parts. For comparability, all the 3D maps from Figure III.1 (exchange energy vs. r_1 and r_2 grid points) are drawn at the same vertical scale.

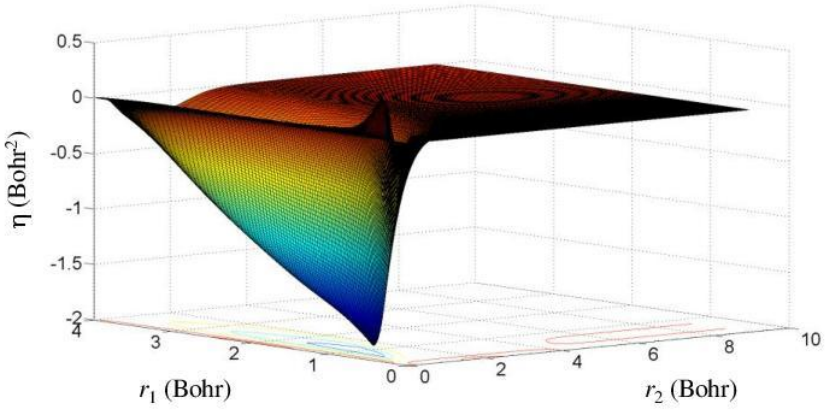

Figure III.2. The grid representation of the quantity defined in equation (III.10).

We propose as interesting quantity the following transformation of Slater-Condon primitives involved in the exchange integrals:

$$u_{ab}(r_1, r_2) = \frac{1}{\rho(r_1)} R_{n_a l_a}(r_1) R_{n_b l_b}(r_1) R_{n_a l_a}(r_2) R_{n_b l_b}(r_2) \frac{min(r_1, r_2)^k}{max(r_1, r_2)^k} r_2^2 \qquad \text{(III.10)}$$

Performing over such terms the above numeric discretization and taking the corresponding summations, as paralleling the obtaining of the total energy, one may obtain profiles (see Figure III.2) that can be interpreted as an object useful in the further quest for new empirical recipes for Fermi hole shape. With the precautional stand demanded when stepping in areas of delicate subjects, one may propose here the idea of redrawing the Fermi hole in atoms as a spherical crust, instead of actual image of local hole in homogenous or non-homogenous electronic density. Analysing sections along the r_2 coordinate in Figure III.2, one may believe that a sharp Gaussian profile of the radial section may be a reasonable approximation. This way, we realised the idea from which we started, represented in the scheme from Figure III.3.

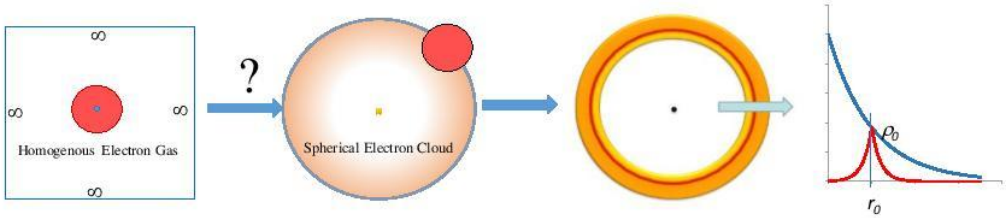

Figura III.3. Synopsis of the resulted paradigma change: the treatment of the Fermi hole it is inadequated for the atoms, violating the spherical symmetry. The right-half of the scheme suggest replacing the hole with a spherical crust with Gaussian profile or Slater.

III.C. Implementation of the new density functional types in an open-source code routine. (Obj. D.2.2.1-D.2.2.2)

The technology used nowadays in electronic structure calculations, based on GTO, eliminated the concept of separability between the radial and angular part of the wave function and also the explicit dependence of the Coulombian, exchange and correlation effects from the Slater-Condon parameters. To discourage the use of the "black box" methods, we implemented the general treatment in Matlab-Octave scripts, accessible in academic format, on demand.

III.D&G. Corelations between the calculated and experimental structural data (molecular geometries, spectra, magnetism). (Obj. D.2.2.3) / Implementation of the new basis set types in an open-source code routine. (Obj. D.2.1.2)

We will continue by revisiting the parameters that are related with the EPR spectroscopy touching the problem of the hyperfine coupling. Particularly important is the case of abundant ^{14}N isotope, having a $I = 1$ nuclear moment. We skip the discussion regarding the g factor, since, in the case of stable nitroxide systems, it does not show spectacular variations, neither in experimental nor in computational respects, remaining almost isotropic and nearby the free electron value[33,34]. Despite being small in the energy scale, the computed hyperfine term is very sensitive to the basis set. Is a truism that all of the computed data depend on the method of choice and selected basis set, but the hyperfine coupling poses quite extreme challenges. Namely, it measures a coupling taking place at the nucleus (between the nuclear spin and the nearby spin density), being also sensitive to long-range effects, like the interactions with the solvent.

Therefore, a basis set accounting for *A* parameters should be accurate both at nucleus and at the outskirts of the atom. Being concerned with the density in the range of the covalent or ionic radii, most of the bases may ignore the details at the nucleus. For this reason, in calculations with Gaussian type orbitals (GTOs), must use special bases, explicitly named EPR-II and EPR-III, when the account of the *A*-type parameters is envisaged. However, we can audaciously claim that practically none of the basis sets in use are taking a proper care of the long-range effects.

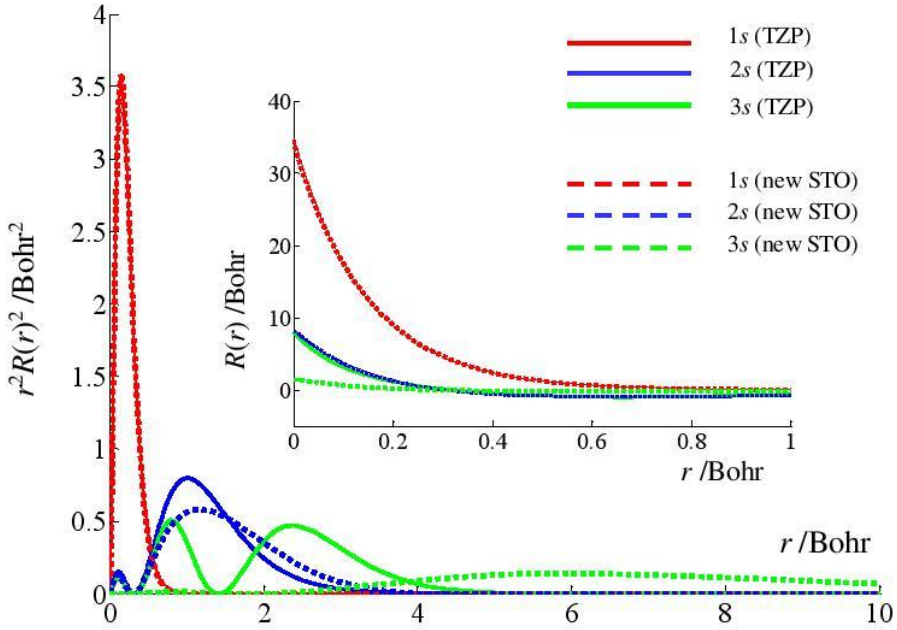

Figure III.4. Radial profiles of the 1s, 2s, and 3s atomic orbitals of the nitrogen, computed with STO-type functions and BLYP functional in the ADF code. The continuous lines correspond to the standard TZP basis, the dashed lines illustrating preliminary tests with a new basis showing long-range maxima in the $r^2R(r)^2$ functions. The inset shows the r vs. $R(r)$ variation near nucleus.

Figure III.4 clearly illustrates that the tentatively new proposed basis shows for the 3s shell (in the r vs. $r^2R(r)^2$ representation) maxima beyond the atomic radius, at about 6 Bohr. The 3s in the standard TZP set of the ADF suite has an average radial extension close to those of the 2s, which is not quite reasonable. The 1s are very similar in the two bases, the 2s profiles having minor mutual differences. The 1s and 2s show similar curves when the two bases are compared in the $R(r)$ function near nucleus. The new 3s, shown with dashed light green in the inset of Figure III.4, has smaller value at $r = 0$ than the 3s from TZP (that here is accidentally coincident with the 2s curve). This is also reasonable, since larger orbits are supposed to have lower amplitudes at low radii. In other words, the density must be invested in the atomic periphery on the expense of lower representation in the inner part. We limited the discussion on the s-type orbitals, because having non-null density at nucleus are directly responsible for the Fermi contact phenomena that determine the isotropic hyperfine coupling.

A deal concerning also the deep orbitals is the case of X-ray photoelectron spectroscopy (XPS). In the continuation of the discussion from the section II.E about the valence-shell-determined spectral terms of the d-type transition metal ions, taking as example the Ni(II) case, we will examine the comparison with XPS prototypic data. The basis set is the same obtained previously, with focus on the d shell, considering now the 2p inner orbitals. The experimental data were obtained by inner cooperation inside our institute (grace to Simona Somacescu), recording the corresponding domain in a nickel oxide sample (NiO with rocksalt structure).

The figure III.5 shows the experimentally recorded XPS profile (continuous line) superposed on the computed orbital energies (marked by bars). The experimental line shows two main formations, assignable to the relativistic $2p_{3/2}$ and $2p_{1/2}$ orbitals, their energy gap corresponding to the spin-orbit coupling parameter. The inner split inside each peak (because of further environmental effects and possible spin-other-orbit couplings) are neglected, considering the experimental barycenters at about 857.8 eV and 880.8 eV for the $2p_{3/2}$ and $2p_{1/2}$, respectively, with a spin-orbit gap ξ_{2p}=23 eV.

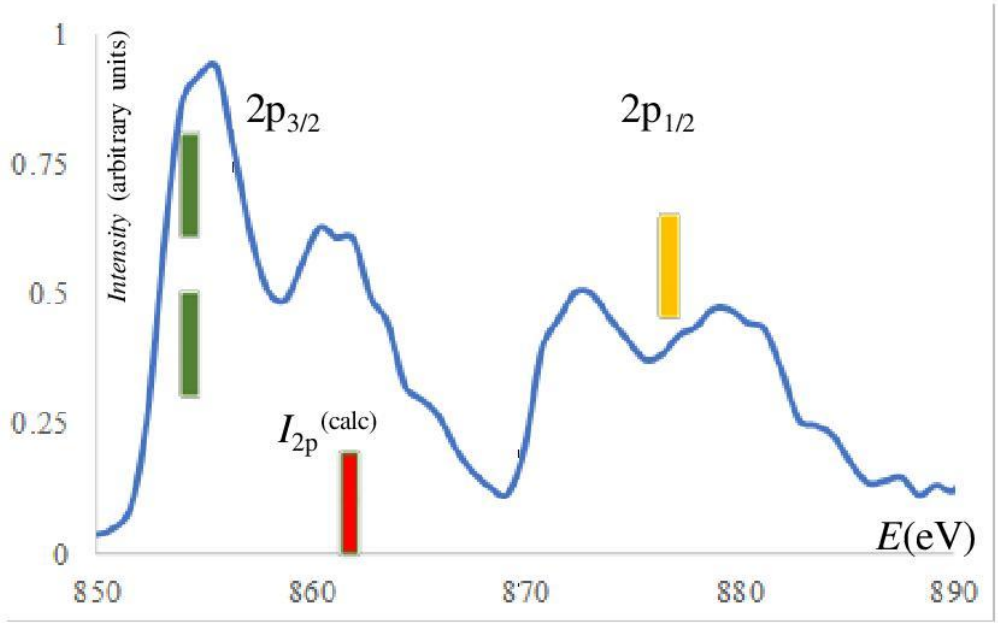

Figure III.5. Experimental XPS data revealing the spin-orbit split inside the 2p shell of the nickel atom in NiO latice, vs. calculated position of non-relativistic ionization potential (I_{2p}) aside the relativistic $2p_{3/2}$ and $2p_{1/2}$ components (marked by bars); The spacing between the $2p_{3/2}$ and $2p_{1/2}$ bars yields the ξ_{2p} spin-orbit coupling parameter.

For the calculation of the spin-orbit coupling parameter in a shell generically denoted by "*a*", we adopt the well-known formula[22]:

$$\xi_a = \alpha^2 \int_{r=0}^{r=\infty} R_a(r) \frac{1}{r} \frac{dV(r)}{dR} R_b(r) r^2 dr \quad , \qquad \text{(III.11)}$$

where α is the fine-structure constant (α=1/137.036 atomic units) and $V(r)$ is the electrostatic potential inside the atomic body. For the here fitted basis set of the nickel atom we obtained the computed ξ_{2p}=22.4 eV, which is in excellent agreement with the experimental evaluation. Although this computation is made for the free ion, it is expected that the long-range environment has a small impact on the gradient of the electric potential and on the radial atomic function, for such inner shell. Besides, it happens that the computed ionization potential (taken as the negative of selfconsistent orbital energy for 2p) falls very well in the range of experimental data. This is more or less fortunate, since here one may hope only for a semi-quantitative agreement. We neglected again the lattice effect. We emphasize that the important result here is the magnitude of the spin-orbit parameter, directly dependent on the quality of the basis set, less influenced by the subtle lattice factors.

III.E&F. The elaboration of the theory of DFT semiempirical varieties, based on atomic body energies as function of charges and populations. (Obj. D.2.2.4)/ The parametrization of the DFT semiempiric theory with atomic spectroscopy data, experimentals and calculated. (Obj. D.2.2.4 si D.2.2.5)

In the following, we will construct a model illustrative for some of the above discussed ideas: energy derivatives, electronegativity, chemical hardness (electrorigidity), states superposition and fractional occupation numbers. Namely, we propose outlining the energies of the atomic bodies as continuous functions of the shell populations. More specifically, since the s^s configuration is a trivial case, the atoms with s^sp^p and $s^sp^pd^d$ valence shells will be considered. The last one, defining transition metal atoms, is isomorphic with the $s^sd^df^f$ case of lanthanides (and actinides). The clue of producing the aimed function of energy is to take the interpolations over spectral states with different shell occupation numbers (integer values), extending the dependence to general fractional populations and continuity.
The simple case of s^s implies the quadratic fit over the energies of the s^2, s^1 and s^0 configurations. This pattern may regard atoms and ions of alkali metals (s^1 atomic groundstates) or alkaline earth elements (s^2 ground configuration).

Now, we move to the case of main group elements, described by *n*s.*n*p valence shells, aiming to design a continuous energy function of s and p shell occupancies, namely for a general s^sp^p configuration. Let us adopt the following notation of configuration types:

$\omega_2= s_2p^{n-2}$, $\omega_1= sp^{n-1}$, $\omega_0= p^n$ (III.12)

the subscript marking the integer occupation of the s shell, while the occupation of p, $p=n-s$, is tuned along with the Q charge of the concerned atom (depending also on the nuclear charge Z). Assuming than we can know the energies of ω_i configurations with i=0, 1, 2 and integer n (detailing later, how), we propose the interpolating function as follows:

$$E(s,p)=C_0(s)E(\omega_0)+C_1(s)E(\omega_1)+C_2(s)E(\omega_2) \qquad \text{(III.13)}$$

The $C_i(s)$ coefficients are doing the interpolation, accounting the fractional population s of the s shell, while the general p value of p is subsequently handled taking polynomial functions of $n=s+p$, fitting over the available integer n cases of the given atom. The conditions imposed over the coefficients are to become 1 if the an integer occupation of s shell equals its indices, while, simultaneously the other two factors are vanishing: $C_i(k)=\delta_{ik}$ for i and k running on 0, 1 and 2. In other words, we want, considering (III.12) and (III.13), to retrieve the tautological relationships $E(s^2p^{n-2})=E(\omega_2)$, $E(s^1p^{n-1})=E(\omega_1)$ and $E(p^n)=E(\omega_0)$. These requirements are met with:

$$C_0(s)=\frac{1}{2}s(s-1)$$
$$C_1(s)=s(2-s) \qquad \text{(III.14)}$$
$$C_2(s)=\frac{1}{2}(s-1)(s-2)$$

Besides, the coefficients obey the following weight properties:

$$\sum_i C_i(s) = 1$$
$$\sum_i i \cdot C_i(s) = s \qquad \text{(III.15)}$$
$$\sum_i i^2 C_i(s) = s^2$$

The $E(\omega_i)$ energies for integer n populations of the valence shells are obtained as average of the spectral terms, as will be illustrated immediately, followed by the fit with a polynomial (at least of second order if more than three points are available). The model can provide atomic energies at fractional s and p occupations, mimicking then, on experimental grounds, what a DFT calculation can do. Taking derivatives, one may obtain electronegativities of s and p shells, their electrorigidities or the inter-shell electrorigidity (the second order derivative with respect of dsdp variation). The spectral terms can also originate from a multi-configurational calculation, the model intermediating then the conversion to a DFT phenomenology. The DFT calculations can directly provide the configuration energies and their derivatives, as will also discuss later for the nitrogen atom, as example.

Now, we will construct the interpolating function for the case of a $s^s p^p d^d$ valence shell, specific to transition metal atoms. The representative configurations are defined as follows:

$\omega_{00} = d^n$, $\omega_{10} = sd^{n-1}$, $\omega_{01} = pd^{n-1}$,

$\omega_{20} = s^2 d^{n-2}$, $\omega_{11} = spd^{n-2}$, $\omega_{02} = p^2 d^{n-2}$, (III.16)

serving as components for the following interpolation:

$$\begin{aligned} E(s,p,d) = {} & C_{00}(s,p)E(\omega_{00}) + C_{10}(s,p)E(\omega_{10}) + C_{01}(s,p)E(\omega_{01}) \\ & + C_{11}(s,p)E(\omega_{11}) + C_{20}(s,p)E(\omega_{20}) + C_{02}(s,p)E(\omega_{02}) \end{aligned} \qquad \text{(III.17)}$$

The coefficients are explicit functions of s and p populations, the dependence on the d=n-s-p being incorporated in the $E(\omega_{ij})$ configurations. The subscripts are marking the situations of integer occupation of s and p shells. The coefficients are obtained from the condition $C_{ij}(k,l)=\delta_{ik}\delta_{jl}$, with for i, j, k and l running on 0, 1 and 2, meaning that the functions becomes the energy of a primitive from the (III.16) set, at corresponding integer occupations of s and p shells. Their expressions are:

$$C_{00}(s,p) = \frac{1}{2}(1-s-p)(2-s-p), \quad C_{11}(s) = sp,$$
$$C_{10}(s,p) = s(2-s-p), \quad C_{20}(s) = \frac{1}{2}s(s-1), \qquad \text{(III.18)}$$
$$C_{01}(s,p) = p(2-s-p), \quad C_{02}(s) = \frac{1}{2}p(p-1).$$

Interestingly, the following regularities are obeyed:

$$\sum_{i+j\le 2} C_{ij} = 1, \qquad \sum_{i+j\le 2} i \cdot j \cdot C_{ij} = s \cdot p,$$
$$\sum_{i+j\le 2} i \cdot C_{ij} = s, \qquad \sum_{i+j\le 2} i^2 C_{ij} = s^2, \qquad \text{(III.19)}$$
$$\sum_{i+j\le 2} j \cdot C_{ij} = p, \qquad \sum_{i+j\le 2} j^2 C_{ij} = p^2.$$

As in the previous case, the energies of primitive configurations, $E(\omega_{ij})$ for integer shell occupations $n=s+p+d$, are found handling experimental data or computations of different sorts, drawing then a polynomial interpolation that renders their continuous dependence on n, equivalent to fractional d occupations, while the fractional s and p are emulated by the (III.18) weighting. The procedure for the transition metal ions can be extended for lanthanides with $s^s d^d f^f$ shell, where, in isomorphic manner, the former role of d is taken by f, while d behaves, algebraically, as the former p shell.

Note that, in the elaborated model, the (III.13) and (III.17) equations correspond to the point that the fractional occupation numbers in DFT are conceived as superposition of states (as averaging, not as configuration interaction).

Now, the atom with $s^s p^p$ configuration will be exemplified, taking the nitrogen atom. The spectral terms are taken from NIST atomic levels database. Generally, each $^{2S+1}[L]$ term splits into spin-orbit J multiplets, $^{2S+1}[L]_J$. Furthermore, we aim a phenomenological model, where the energies of a configuration is defined as average of all the $^{2S+1}[L]$ terms arising from a certain ω configuration, e.g. one from the list (III.12) or (III.15). In this view, the term energies are weighted with their total, orbital and spin multiplicity, $(2L+1)\,(2S+1)$, having:

$$E(\omega)=\frac{\sum_{L,S}(2L+1)(2S+1)E\left(^{2S+1}[L]\in\omega\right)}{\sum_{L,S}(2L+1)(2S+1)} \qquad \text{(III.20)}$$

The databases for a given charge of the atom are reporting the levels with respect of its groundstate. For our purpose, we need that any term to be related to a unique convened level, the neutral atom, for instance. Then, the terms of positive ions must be shifted with the sum of the spectral limits of all the previous charge states, down to the neutral atom. The spectral limit is the value representing the ionization energy of the groundstate, bringing it to the groundstate of the atom incremented with one more positive charge.

Table 3.1. Available spectral terms for nitrogen atom, at Q=0, with respect of parent configurations and subsequent handling by averaging and energy shift. The first line gives the groundterm, while the last one, the spectral limit. All values are in cm^{-1}.

Cfgs.	Terms	Average over J multiplets	Relative to neutral N groundstate	Configuration averaged energy (vs N^0 groundstate)	Relative to $2s^2.2p^3$ average
	^4S	0	0		
$2s^2.2p^3$	^4S	0	0	18266	0
$2s^2.2p^3$	^2D	19228	19228		
$2s^2.2p^3$	^2P	28839	28839		
$2s.2p^4$	^4P	88129	88129	103161	84896
$2s.2p^4$	^2D	121201	121201		
Limit		117356			

The Tables 3.1 and 3.2 are illustrating the data for the series of nitrogen atom with charges 0 and +1. The first line of the table gives the ground term of each system. After averaging over the J multiplets, the term value may result slightly shifted from local zero, as is the case of ^3P in Table 3.2, the 103 cm^{-1} value resulting from the weighting of 0, 49 and 131 cm^{-1}, for the J=0, 1 and 2. Another shift occurs at the end, given in the last column of each table, subtracting the average of $2s^2.2p^3$ configuration, itself shifted from zero, because of

incorporated ^{2}P and ^{2}D excited terms. Taking an average over different spin states represents a conventional limit of the model, obtaining then an enforced restricted spinless picture. Namely, each $s^s p^p$ configuration is tacitly considered as half spin-up, $s^{s\alpha/2}p^{p\alpha/2}$ plus half spin-down, $s^{s\beta/2}p^{p\beta/2}$.

Table 3.2. Available spectral terms for nitrogen atom, at Q=1, with respect of parent configurations and subsequent handling by averaging and energy shift. The first line gives the groundterm, while the last one, the spectral limit. All values are in cm^{-1}.

Cfgs.	Terms	Average over J multiplets	Relative to neutral N groundstate	Configuration averaged energy (vs N^0 groundstate)	Relative to $2s^2.2p^3$ average
	$^3P_0$	0	117356		
$2s^2.2p^2$	^3P	103	117460	124703	106438
	^1D	15316	132673		
	^1S	32689	150045		
$2s.2p^3$	^5S	46785	164141	224535	206270
	^3D	92244	209600		
	^3P	109217	226574		
	^1D	144188	261544		
	^3S	155127	272483		
	^1P	166766	284122		
$2p^4$	^3P	220293	337650	337650	319384
Limit		238750			

The further step is fitting the available data with a convenient polynomial. The operation is illustrated in the Figure III.6. Certain configurations are not findable at some charges, as is the ω_0 for the neutral atom, e.g. the p^5 case. Or, the ω_2 is impossible at Q=4, since the system has only one electron. Also, there are no data on the negative ions. Having for each series at least four available points, the data can be fitted with cubic polynomials, the results being shown as continuous lines, passing through the marked points of the left panel, and extrapolated for negative charges of the atom.

The experimental information is complemented with computed configuration energies, represented in the right side of the Figure III.6. To be distinguished from experiment, now, all the possible configurations, with total population ranging from n=0 (Q=5) to n=8 (Q=-3) can be obtained. A very suited code is the ADF (Amsterdam Density Functional), since it allows controlling explicitly the orbital populations, using fractional occupations and emulating the spinless restricted convention. As one may see, comparing the two sides of the Figure III.6, the calculation is well paralleling the available experimental data and simulates the unknown part in a way that seems better than the extrapolations from experiment. This is noticeable particularly considering that the simplest functional was used, the LDA, altogether with a basis set of average quality (TZP). With the discussed model and data, we can do several numeric experiments. The Figure III.7 shows, in the right side, a verification of the Janak theorem: it finds a series of lines with slope practically equal to the unity, when draw orbital energies, as resulted directly from the DFT calculations against the derivatives performed with the continuous energy model. There are six curves, three corresponding to the s shell, from the ω_i (i=0,1,2) configurations, at integer charges from Q=-3 to +5, and three for the p shell. The lines are practically superposed and the points not well visible, in their series, but we aim here to see the global fulfilment of the correlation, not judging each curve.

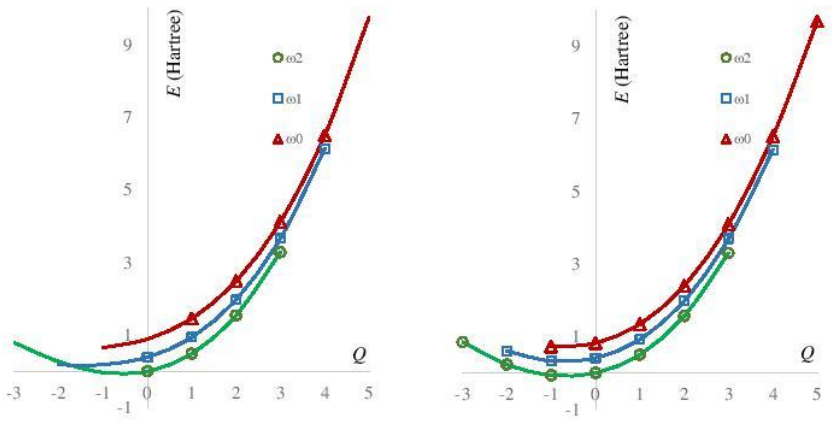

Figure III.6 The energies of $\omega_2 = s^2p^{n-2}$, $\omega_1 = sp^{n-1}$ and $\omega_0 = p^n$ configurations for the nitrogen atom. Left panel: available data from experiment. The marked points are the values collected from Tables 1.A-1.E, converted to atomic units (Hartree), while the lines represent their fit by cubic polynomials, as function of total shell population (n) or atom charge Q. Right side panel: the configurations computed directly in DFT, with ADF code (LDA functional, TZP basis set).

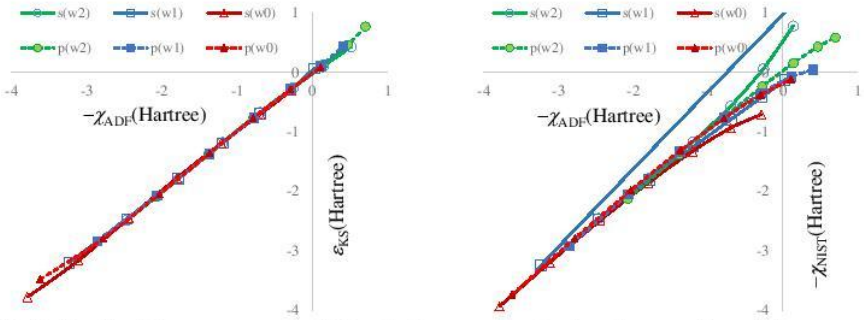

Figure III.7. Left side: The assessment of Janak theorem, retrieving the equality of the energy derivatives (ascribed as negative of electronegativity, $-\chi$) with the actual ε_{KS} energies for 2s and 2p shells, both based on LDA/TZP calculations with ADF code. Right side: comparison of energy derivatives (labelled as $-\chi$) with data from DFT-ADF calculation versus the interpolation to experimental points (NIST).

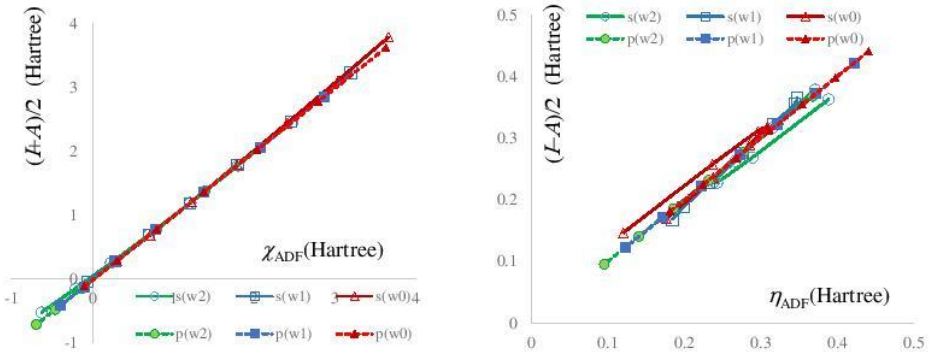

Figure III.8. The comparison of electronegativity (left side) and hardness (right side) computed as energy derivatives (abscissas) versus Mulliken-type approximations (half-sum and half-difference of ionization potentials and electron affinities). All the data are coming from the DFT calculation with the ADF code.

The right side panel compares the derivatives from the direct DFT calculation with the model based on NIST points. One may conclude a good match, the deviations appearing nearby the points that fall in extrapolation regime, in the experiment-based model, especially in the upper-right corner, which corresponds to weak orbital stabilization, or even positive energies of the shells in negatively charged systems. This analysis is relevant, because there are no primary experimental data which can be directly compared with Kohn-Sham orbital energies, needing the interim support of a model like the here presented one. To the best of our knowledge, this is an unprecedented illustration of such a basic problem.

In the Figure III.8 we are checking the validity of Mulliken approximation for electronegativity and the related form for *electrorigidity*. For this purpose we used only the calculated data, since we aim to verify a consistence of theory with itself and, besides, in this way we have more accounted points than in the experimental limit. The ionisation and affinity of the s shell is done with the help of (III.13) function, as the following differences: $I_s(s,p)=E(s-1,p)-E(s,p)$ and $A_s(s,p)=E(s,p)-E(s+1,p)$, these being regarded also as continuous functions. The p analogues are $I_p(s,p)=E(s,p-1)-E(s,p)$ and $A_p(s,p)=E(s,p)-E(s,p+1)$. There are zones where the definitions are not nominally valid: e.g. the ionization of s from fractional configurations with $s<1$ would lead to negative populations, while the affinity for $s>1$ would represent an impossible configuration, with more than two electrons in the s orbital. However, the non-physical margins can be formally ignored, once are used to produce approximations to derivative functions that are allowed in the whole $0<s<2$ interval. The left side from Figure III.8 proves that the electronegativity (taken as derivative of total energy) is very well approximated by the $(I+A)/2$ formula, for all the possible situations. The six lines (two shells for each of the three types of configurations) are all superposed as a diagonal slope. Is not important that series are not well visible individually, the point to be retained being the overall, approximate but good, validity of the Mulliken formula. The $(I-A)/2$ representations against the second order derivatives for the s and p shell shows a slight deviation from the unitary slope. This is normal, since the higher derivatives are expected to carry more advanced details of the intimate electron structure, mimicked with lesser extend by finite difference approximations. However, the correlation is good, validating then the convenient and simple Mulliken-type approximations to electronegativity and electrorigidity.

Conclusion

We approached the issue of revisiting the basic issues of basis sets, assessing prototypic cases from the beginning and the end of periodic table. Namely, the account of orbital energies of the H atom with the existing stock of Gaussian Type Orbitals was exhaustively mapped, concluding a quasi-general unsatisfactory performance, prompting us for the future improvement. On the other side, the basis sets for the f shell of lanthanides were produced with the help of plane-wave methods, considering that this frame can be extrapolated to the infinite dimension. Specific properties of lanthanide atoms in molecules, ligand field and exchange coupling parameters were discussed, whose computation account is implicitly determined by the quality of f-shell basis sets.

We continued with the elaboration of a new theory and the corresponding algorithm for the treatment of the spherical mediated atom, within the wave-function and density functional theories. The review of he basis sets continued with series of atoms and ions of different types: non-metals, transitional d and lanthanides, presenting new principles and results, both in Gaussian and Slater formats. Special attention was paid to fine tuning the bases, to reproduce excited states and related parameters, Slater-Condon or Racah. Applications in spectroscopy and magnetism are presented. The whole process involved a significant effort in writing new codes, covering the methodological issues developed.

We invented a new principle to construct and analyze density functionals, obeying the spherical symmetry of the atomic bodies. Besides, a new phenomenological version of density functional theory was designed, which can be based on experimental spectroscopic data, or with alternative calculations from wave-function-theories. Corroborated with the drastic revision of principles and methods concerning the orbital atomic bases, we realized interesting breakthroughs which have to be further consolidated in future works.

*
**
***
****

Appendix

Table I.A1. Orbital energies (in Hartree) for H atom, taken by an extended series of GTO bases.

n	1	2	3	4	5	6	
Exact	**-0.5000**	**-0.1250**	**-0.0556**	**-0.0313**	**-0.0200**	**-0.0139**	etc
STO-2G	**-0.4544**						
STO-3G	**-0.4666**						
STO-6G	**-0.4710**						
3-21G	**-0.4962**	0.5865					
3-21GSP	**-0.4970**	0.3739					
3-21++G	**-0.4978**	**-0.1154**	0.7329				
4-31G	**-0.4982**	0.4609					
4-22GSP	**-0.4993**	1.8297					
6-31G	**-0.4982**	0.4609					
6-31G*	**-0.4982**	0.4609					
6-31G**	**-0.4982**	0.4609	1.6342				
6-31+G	**-0.4982**	0.4609					
6-31+G*	**-0.4982**	0.4609					
6-31+G**	**-0.4982**	0.4609	1.6342				
6-31++G	**-0.4988**	**-0.1164**	0.6184				
6-31++G*	**-0.4988**	**-0.1164**	0.6184				
6-31++G**	**-0.4988**	**-0.1164**	0.6184	1.6342			
6-31++G**-J	**-0.4996**	**-0.1166**	0.4537	1.6342	4.2383	34.2144	
6-31G(2df,p)	**-0.4982**	0.2806	0.4609	3.3265			
6-31G(3df,3pd)	**-0.4982**	0.0067	0.4609	1.3796	2.6489	7.7471	
6-311G	**-0.4998**	0.0259	1.8865				
6-311G*	**-0.4998**	0.0259	1.8865				
6-311G**	**-0.4998**	0.0259	0.9537	1.8865			
6-311+G	**-0.4998**	0.0259	1.8865				
6-311++G	**-0.4998**	**-0.1188**	0.1797	2.0356			
6-311+G*	**-0.4998**	0.0259	1.8865				
6-311+G**	**-0.4998**	0.0259	0.9537	1.8865			
6-311++G*	**-0.4998**	**-0.1188**	0.1797	2.0356			
6-311++G**	**-0.4998**	**-0.1188**	0.1797	0.9537	2.0356		
6-311+G(2d,p)	**-0.4998**	0.0259	0.9537	1.8865			
6-311++G(2d,2p)	**-0.4998**	**-0.1188**	0.1797	0.2806	2.0356	3.3265	
6-311++G(3df,3pd)	**-0.4998**	**-0.1188**	0.0067	0.1797	1.3796	2.0356	
6-311G(2df,2pd)	**-0.4998**	0.0259	0.2806	1.8865	2.6489	3.3265	
MINI (Huzinaga)	**-0.4970**						
MINI (Scaled)	**-0.4659**						
MIDI (Huzinaga)	**-0.4970**	0.3741					
MIDI!	**-0.4970**	0.3741					
SV (Dunning-Hay)	**-0.4976**	0.5267					

SVP (Dunning-Hay)	**-0.4976**	0.5267	1.4362				
SVP + Diffuse (Dunning-Hay)	**-0.4993**	**-0.1023**	0.7406	1.4362			
DZ (Dunning)	**-0.4976**	0.5267					
DZP	**-0.4991**	0.1530	1.0543				
DZP (Dunning)	**-0.4976**	0.5267	1.4362				
DZP + Diffuse (Dunning)	**-0.4993**	**-0.1023**	0.7406	1.4362			
DZP-DKH	**-0.4991**	0.1455	1.0543				
DZVP (DFT)	**-0.4982**	0.4165					
DZVP2 (DFT)	**-0.4982**						
Ahlrichs VDZ	**-0.4993**	0.1817					
Ahlrichs pVDZ	**-0.4993**	0.1817	1.0485				
Ahlrichs VTZ	**-0.4998**	0.0271	1.8981				
ADZP	**-0.4991**	**-0.1231**	**-0.0379**	0.2770	1.3698		
ATZP	**-0.4998**	**-0.1233**	**-0.0950**	0.1612	0.3834	0.4502	etc
AQZP	**-0.5000**	**-0.1231**	**-0.1037**	0.1660	0.2262	0.3631	etc
A5ZP	**-0.5000**	**-0.1244**	**-0.0825**	0.0721	0.1634	0.3595	etc
IGLO-II	**-0.4998**	0.0213	0.7673	1.8494			
IGLO-III	**-0.4999**	**-0.0462**	0.2100	0.8126	2.8174	5.3558	
ANO-RCC	**-0.5000**	**-0.1231**	**-0.0905**	0.0848	0.3924	0.5052	etc
Roos Augmented Double Zeta ANO	**-0.4999**	**-0.1201**	**-0.0438**				
Roos Augmented Triple Zeta ANO	**-0.5000**	**-0.1209**	**-0.0779**	0.4219	0.6171	0.8124	etc
Sadlej pVTZ	**-0.4998**	**-0.1208**	**-0.0885**	0.2401	0.5754		
Sadlej+	**-0.4998**	**-0.1246**	**-0.1094**	**-0.0547**	**-0.0442**	**-0.0247**	etc
SBKJC (p,2d)	**-0.4978**	**-0.0874**	**-0.0792**	0.8377	4.9982		
SBKJC VDZ ECP	**-0.4962**	0.5865					
LANL2DZ ECP	**-0.4976**						
LANL2DZdp ECP	**-0.4993**	**-0.1004**	0.2552	0.7478			
CRENBL ECP	**-0.4993**	0.1205	2.6702	21.7667			
Def2-SV(P)	**-0.4993**	0.1817					
Def2-SVP	**-0.4993**	0.1817	1.0485				
Def2-SVPD	**-0.4993**	**-0.0735**					
Def2-TZVP	**-0.4998**	0.0271	1.0485	1.8981			
Def2-TZVPD	**-0.4998**	**-0.0927**	0.0271	1.2027	1.8981		
Def2-TZVPP	**-0.4998**	0.0271	0.2985	1.8981	2.8245	3.1992	
Def2-TZVPPD	**-0.4998**	**-0.0923**	0.0271	0.5376	1.8981	2.8245	etc
Def2-QZVP	**-0.5000**	**-0.0525**	0.1359	0.7307	1.5534	1.8026	etc
Def2-QZVPD	**-0.5000**	**-0.1015**	**-0.0525**	0.3599	0.7307	1.5534	etc
Def2-QZVPP	**-0.5000**	**-0.0525**	0.1359	0.7307	1.5534	1.8026	etc
Def2-QZVPPD	**-0.5000**	**-0.1015**	**-0.0525**	0.3599	0.7307	1.5534	etc
cc-pVDZ	**-0.4993**	0.1819	0.9104				
cc-pVDZ-F12	**-0.4998**	0.0258	0.1414	1.8863	2.3221		

cc-pVDZ-F12 MP2 Fit	**-0.4992**	0.0329	0.2448	0.9623	1.3875	1.8923	etc
cc-pVDZ-F12_OPTRI	**-0.4912**	0.3931	0.7874	1.0003	3.9845	4.6009	etc
cc-pVDZ-fit2-1	**-0.4995**	**-0.1232**	**-0.0633**	0.0186	0.2159	0.3371	etc
cc-pVDZ-RI	**-0.4802**	1.0214	1.1876	3.1809	6.0417	8.5253	
cc-pVTZ	**-0.4998**	0.0258	0.2985	1.8863	2.8245	3.1992	
cc-pVTZ-F12	**-0.4999**	**-0.0239**	0.0155	1.0091	1.0466	1.0920	etc
cc-pVTZ-F12 MP2 Fit	**-0.4971**	0.1512	0.1742	0.4522	1.2970	1.6761	etc
cc-pVTZ-F12_OPTRI	**-0.4942**	0.1590	0.2599	0.5422	2.4530	2.4753	etc
cc-pVTZ-fit2-1	**-0.4998**	**-0.1241**	**-0.0993**	0.0014	0.0586	0.2345	etc
cc-pVTZ-RI	**-0.4823**	0.5016	0.5145	2.5279	3.1536	3.3391	etc
cc-pV(T+d)Z+	**-0.4998**	0.0258	0.2985	1.8863	2.8245	3.1992	
cc-pVQZ	**-0.4999**	**-0.0239**	0.1359	1.0091	1.5534	1.8026	etc
cc-pVQZ-F12	**-0.5000**	**-0.0729**	**-0.0129**	0.5255	0.6936	0.8703	etc
cc-pVQZ-F12 MP2 Fit	**-0.4994**	**-0.0313**	0.0631	0.6508	0.7024	1.0746	etc
cc-pVQZ-F12_OPTRI	**-0.4788**	0.6313	0.7743	1.1684	3.5389	4.8766	etc
cc-pVQZ-RI	**-0.4933**	0.0325	0.3014	1.0349	1.0482	2.2041	etc
cc-pV5Z	**-0.5000**	**-0.0729**	0.0681	0.5255	1.0126	1.3290	etc
cc-pV5Z-RI	**-0.4933**	0.1587	0.3080	1.0848	1.5672	1.8068	etc
cc-pV6Z	**-0.5000**	**-0.0957**	0.0250	0.3026	0.6929	1.0557	etc
cc-pV6Z-RI	**-0.4995**	**-0.0152**	**-0.0008**	0.6383	0.7164	0.7670	etc
cc-pV8Z	**-0.5000**	**-0.1091**	**-0.0460**	0.1822	0.4655	0.5892	etc
aug-cc-pVDZ	**-0.4993**	**-0.1219**	**-0.0479**	0.3185	1.2144		
aug-cc-pVDZ_OPTRI	**-0.4903**	**-0.0242**	0.1225	1.4415	1.8462	2.3176	etc
aug-cc-pVTZ	**-0.4998**	**-0.1240**	**-0.0869**	0.1387	0.4356	0.5574	etc
aug-cc-pVTZ_OPTRI	**-0.4880**	0.3390	0.7808	1.4136	2.8398	5.1228	etc
aug-cc-pVQZ	**-0.4999**	**-0.1244**	**-0.1010**	0.0850	0.2842	0.3622	etc
aug-cc-pVQZ_OPTRI	**-0.4952**	0.2299	0.4999	0.8309	2.8120	2.9838	etc
aug-cc-pV5Z	**-0.5000**	**-0.1248**	**-0.1083**	0.0271	0.1979	0.2715	etc
aug-cc-pV5Z_OPTRI	**-0.4773**	0.7687	1.2259	1.6821	1.8836	4.5608	etc
aug-cc-pV6Z	**-0.5000**	**-0.1249**	**-0.1127**	**-0.0015**	0.1282	0.2115	etc
aug-mcc-pVTZ	**-0.4998**	**-0.1246**	**-0.0879**	0.1121	0.4367	0.5556	etc
aug-mcc-pVQZ	**-0.4999**	**-0.1247**	**-0.1024**	0.0641	0.2786	0.3577	etc
aug-mcc-pV5Z	**-0.5000**	**-0.1248**	**-0.1083**	0.0271	0.1979	0.2715	etc
aug-mcc-pV6Z	**-0.5000**	**-0.1246**	**-0.1133**	0.0089	0.1235	0.2041	etc
aug-mcc-pV7Z	**-0.5000**	**-0.1246**	**-0.1156**	**-0.0049**	0.0779	0.1695	etc
aug-mcc-pV8Z	**-0.5000**	**-0.1247**	**-0.1195**	**-0.0293**	0.0796	0.1075	etc
aug-pc-0	**-0.4964**	0.3239					
aug-pc-1	**-0.4986**	0.1313	1.4362				
aug-pc-2	**-0.4999**	**-0.0554**	0.3977	1.1427	3.4235	3.7542	
aug-pc-3	**-0.5000**	**-0.1037**	0.0142	0.2950	1.0691	1.5122	etc
aug-pc-4	**-0.5000**	**-0.1140**	**-0.0437**	0.1641	0.5226	0.7139	etc
pc-0	**-0.4964**	0.3239					
pc-1	**-0.4986**	0.1313	1.4362				
pc-2	**-0.4999**	**-0.0554**	0.3977	1.1427	3.4235	3.7542	
pc-3	**-0.5000**	**-0.1037**	0.0142	0.2950	1.0691	1.5122	etc

pc-4	**-0.5000**	**-0.1140**	**-0.0437**	0.1641	0.5226	0.7139	etc
pcS-0	**-0.4965**	0.3190					
pcS-1	**-0.4987**	0.1292	1.4803				
pcS-2	**-0.4999**	**-0.0552**	0.3990	1.1247	3.4235	3.8450	
pcS-3	**-0.5000**	**-0.1037**	0.0142	0.2951	1.0701	1.5122	etc
pcS-4	**-0.5000**	**-0.1140**	**-0.0437**	0.1641	0.5226	0.7140	etc
pcseg-0	**-0.4964**	0.3239					
pcseg-1	**-0.4986**	0.1313	1.4362				
pcseg-2	**-0.4999**	**-0.0553**	0.3977	1.1434	3.4235	3.7542	
pcseg-3	**-0.5000**	**-0.1032**	0.0142	0.3040	1.0691	1.5122	etc
pcseg-4	**-0.5000**	**-0.1141**	**-0.0437**	0.1673	0.5226	0.7139	etc
pcSseg-0	**-0.4964**	0.3239					
pcSseg-1	**-0.4986**	0.1313	1.4803				
pcSseg-2	**-0.4999**	**-0.0553**	0.3990	1.1434	3.4235	3.8450	
pcSseg-3	**-0.5000**	**-0.1032**	0.0142	0.3040	1.0701	1.5122	etc
pcSseg-4	**-0.5000**	**-0.1141**	**-0.0437**	0.1673	0.5226	0.7140	etc
pcemd-2	**-0.4995**	0.0892	3.0773	3.5674			
pcemd-3	**-0.5000**	**-0.1144**	0.1630	1.0902	3.5674	4.1774	etc
pcemd-4	**-0.5000**	**-0.1250**	**-0.0534**	0.0301	0.3586	0.5799	etc
aug-pcS-0	**-0.4965**	**-0.1225**	0.4345				
aug-pcS-1	**-0.4987**	**-0.1232**	**-0.1051**	0.2496	1.5651		
aug-pcS-2	**-0.4999**	**-0.1246**	**-0.1127**	0.0502	0.0582	0.5334	etc
aug-pcS-3	**-0.5000**	**-0.1249**	**-0.1181**	**-0.0099**	0.0297	0.1712	etc
aug-pcS-4	**-0.5000**	**-0.1250**	**-0.1199**	**-0.0259**	0.0166	0.1063	etc
aug-pcseg-0	**-0.4964**	**-0.1185**	0.4715				
aug-pcseg-1	**-0.4986**	**-0.1230**	**-0.1036**	0.2560	1.5262		
aug-pcseg-2	**-0.4999**	**-0.1246**	**-0.1128**	0.0500	0.0580	0.5320	etc
aug-pcseg-3	**-0.5000**	**-0.1249**	**-0.1181**	**-0.0094**	0.0295	0.1709	etc
aug-pcseg-4	**-0.5000**	**-0.1250**	**-0.1199**	**-0.0260**	0.0164	0.1061	etc
aug-pcSseg-0	**-0.4964**	**-0.1185**	0.4715				
aug-pcSseg-1	**-0.4986**	**-0.1230**	**-0.1035**	0.2560	1.5709		
aug-pcSseg-2	**-0.4999**	**-0.1246**	**-0.1128**	0.0500	0.0580	0.5332	etc
aug-pcSseg-3	**-0.5000**	**-0.1249**	**-0.1181**	**-0.0094**	0.0295	0.1710	etc
aug-pcSseg-4	**-0.5000**	**-0.1250**	**-0.1199**	**-0.0260**	0.0164	0.1061	etc
2ZaPa-NR	**-0.4993**	**-0.1209**	0.4265	1.0698			
3ZaPa-NR	**-0.4999**	**-0.1243**	**-0.0785**	0.1151	0.6444	1.8782	etc
4ZaPa-NR	**-0.5000**	**-0.1250**	**-0.0868**	**-0.0472**	0.1625	0.3628	etc
5ZaPa-NR	**-0.5000**	**-0.1250**	**-0.0970**	**-0.0493**	0.1022	0.2296	etc
6ZaPa-NR	**-0.5000**	**-0.1250**	**-0.1047**	**-0.0518**	0.0698	0.1946	etc
7ZaPa-NR	**-0.5000**	**-0.1250**	**-0.1021**	**-0.0521**	0.0590	0.2105	etc
G3LargeXP	**-0.4998**	**-0.1188**	0.1797	0.2806	2.0356	3.3265	
G3MP2large	**-0.4998**	**-0.1188**	0.1797	0.2806	2.0356	3.3265	
G3MP2LargeXP	**-0.4998**	**-0.1188**	0.1797	0.2806	2.0356	3.3265	

Anexa II. Exemplu de cod Matlab-Octave pentru Wave-Function Theory (WFT) a atomului sferic mediat cu baze GTO generalizate.

```
function etot=
hfmat1gto1(Z,nbas,nocc,bas,cgto,cmo0,ps,pp,pd,pf)
t0=cputime
nprim=length(bas(:,1));
ns=nbas(1);np=nbas(2);nd=nbas(3);nf=nbas(4);
nsocc=nocc(1);npocc=nocc(2);ndocc=nocc(3);nfocc=no
cc(4); nprims=0; nprimp=0; nprimd=0; nprimf=0;
    for iprim=1:nprim
lshell=bas(iprim,2);
if lshell==0
nprims=nprims+1;
sbas(nprims,1)=bas(iprim,1);
sbas(nprims,2)=bas(iprim,2);
sbas(nprims,3)=bas(iprim,3);
end
if lshell==1
nprimp=nprimp+1;
pbas(nprimp,1)=bas(iprim,1);
pbas(nprimp,2)=bas(iprim,2);
pbas(nprimp,3)=bas(iprim,3);
end
if lshell==2
nprimd=nprimd+1;
dbas(nprimd,1)=bas(iprim,1);
dbas(nprimd,2)=bas(iprim,2);
dbas(nprimd,3)=bas(iprim,3);
end
if lshell==3
nprimf=nprimf+1;
fbas(nprimf,1)=bas(iprim,1);
fbas(nprimf,2)=bas(iprim,2);
fbas(nprimf,3)=bas(iprim,3);
end; end
cgtos=cgto(1:nprims,1:ns);
cgtop=cgto(nprims+1:nprims+nprimp,ns+1:ns+np);
cgtod=cgto(nprims+nprimp+1:nprims+nprimp+nprimd,
ns+np+1:ns+np+nd);
cgtof=cgto(nprims+nprimp+nprimd+1:nprims+nprimp+
nprimd+nprimf,ns+np+nd+1:ns+np+nd+nf);
cmo0s=cmo0(1:ns,1:ns);
cmo0p=cmo0(ns+1:ns+np,ns+1:ns+np);
cmo0d=cmo0(ns+np+1:ns+np+nd,ns+np+1:ns+np+nd);
cmo0f=cmo0(ns+np+nd+1:ns+np+nd+nf,ns+np+nd+1:ns+np
+nd+nf);
cs1=cgtos*cmo0s; cp1=cgtop*cmo0p;
cd1=cgtod*cmo0d;cf1=cgtof*cmo0f;
disp('calcul hmat0s')
disp(cputime-t0)
if ns>0
for i=1:nprims
n1=sbas(i,1);a1=sbas(i,3);
nrmgtos(i)=sqrt((2^(3/2+n1)*a1^(1/2+n1))/gamma(1/2
+n1));
end
for i=1:nprims     for j=1:i
n1=sbas(i,1);a1=sbas(i,3);
n2=sbas(j,1);a2=sbas(j,3);
l=0;s=(gamma((1/2)*(n1+n2+1))/(a1+a2)^((1/2)*(n1+n
2+1)))*
sqrt(((2*a1)^(n1+1/2)*(2*a2)^(n2+1/2))/(gamma(n1+1
/2)* gamma(n2+1/2)));
fh=(1/(2*(a1+a2)^((1/2)*(n1+n2+3))))*
sqrt(((2*a1)^(n1+1/2)*(2*a2)^(n2+1/2))
/(gamma(n1+1/2)*gamma(n2+1/2)));
hk0=(a2^2*(l+l^2+n1-n1^2)+a1*a2*
(-l+2*l+2*l^2+n1+n2+2*n1*n2)+a1^2*(l+l^2+n2-
2^2))*gamma((1/2)*(-l+n1+n2));
v0=-2*Z*(a1+a2)^(3/2)*gamma((n1+n2)/2);
h=(hk0+v0)* fh;
hmat0s(i,j)=h; smat0s(i,j)=s;
hmat0s(j,i)=h; smat0s(j,i)=s;end; end
 [csn,esn]=eig(hmat0s,smat0s);
csn=csn'; end
if np>0
for i=1:nprimp
n1=pbas(i,1);a1=pbas(i,3);
nrmgtop(i)=sqrt((2^(3/2+n1)*a1^(1/2+n1))/gamma(1/
2+n1)); end
for i=1:nprimp;     for j=1:i
n1=pbas(i,1);a1=pbas(i,3);
n2=pbas(j,1);a2=pbas(j,3);
l=1;
s=(gamma((1/2)*(n1+n2+1))/(a1+a2)^((1/2)*
(n1+n2+1)))*sqrt(((2*a1)^(n1+1/2)*(2*a2)^
(n2+1/2))/(gamma(n1+1/2)*gamma(n2+1/2)));
fh=(1/(2*(a1+a2)^((1/2)*(n1+n2+3))))*
sqrt(((2*a1)^(n1+1/2)*(2*a2)^(n2+1/2))/
(gamma(n1+1/2)*gamma(n2+1/2)));
hk0=(a2^2*(l+l^2+n1-n1^2)+a1*a2*(-
l+2*l+2*l^2+n1+n2+2*n1*n2)+a1^2*(l+l^2+n2-n2^2))*
gamma((1/2)*(-l+n1+n2));
v0=-2*Z*(a1+a2)^(3/2)*gamma((n1+n2)/2);
h=(hk0+v0)* fh;
hmat0p(i,j)=h; smat0p(i,j)=s;
hmat0p(j,i)=h; smat0p(j,i)=s;
end; end
[cpn,epn]=eig(hmat0p,smat0p);
cpn=cpn';
end
if nd>0
for i=1:nprimd
n1=dbas(i,1);a1=dbas(i,3);
nrmgtod(i)=sqrt((2^(3/2+n1)*a1^(1/2+n1))
/gamma(1/2+n1));
end
for i=1:nprimd
    for j=1:i
n1=dbas(i,1);a1=dbas(i,3);
n2=dbas(j,1);a2=dbas(j,3);
l=2;
s=(gamma((1/2)*(n1+n2+1))/(a1+a2)^((1/2)
*(n1+n2+1)))*sqrt(((2*a1)^(n1+1/2)*(2*a2)
^(n2+1/2))/(gamma(n1+1/2)*gamma(n2+1/2)));
fh=(1/(2*(a1+a2)^((1/2)*(n1+n2+3))))
*sqrt(((2*a1)^(n1+1/2)*(2*a2)^(n2+1/2))
/(gamma(n1+1/2)*gamma(n2+1/2)));
fh=(1/(2*(a1+a2)^((1/2)*(n1+n2+3))))*
sqrt(((2*a1)^(n1+1/2)*(2*a2)^(n2+1/2))
/(gamma(n1+1/2)*gamma(n2+1/2)));
v0=-2*Z*(a1+a2)^(3/2)*gamma((n1+n2)/2);
h=(hk0+v0)* fh;
hmat0d(i,j)=h; smat0d(i,j)=s;
hmat0d(j,i)=h; smat0d(j,i)=s;
end
end
[cdn,edn]=eig(hmat0d,smat0d);
cdn=cdn';
end
if nf>0
for i=1:nprimf
n1=fbas(i,1);a1=fbas(i,3);
nrmgtof(i)=sqrt((2^(3/2+n1)*a1^(1/2+n1))/gamma(1/
2+n1)); end
for i=1:nprimf
    for j=1:i
n1=fbas(i,1);a1=fbas(i,3);
n2=fbas(j,1);a2=fbas(j,3); l=3;
s=(gamma((1/2)*(n1+n2+1))/(a1+a2)^((1/2)*(n1+n2+1
)))*
sqrt(((2*a1)^(n1+1/2)*(2*a2)^(n2+1/2))/(gamma(n1+
1/2) *gamma(n2+1/2)));
```

```
fh=(1/(2*(a1+a2)^((1/2)*(n1+n2+3))))*sqrt(((2*a1)^
(n1+1/2)*(2*a2)^(n2+1/2))/(gamma(n1+1/2)
*gamma(n2+1/2)));
hk0=(a2^2*(1+l^2+n1-n1^2)+a1*a2*(-1+2*l+2*l
^2+n1+n2+2*n1*n2)+a1^2*(1+l^2+n2-n2^2))
*gamma((1/2)*(-1+n1+n2));
v0=-2*Z*(a1+a2)^(3/2)*gamma((n1+n2)/2);
h=(hk0+v0)* fh;
hmat0f(i,j)=h; smat0f(i,j)=s;
hmat0f(j,i)=h; smat0f(j,i)=s;
end; end
[cfn,efn]=eig(hmat0f,smat0f);
cfn=cfn';
end
csn=cs1'; cpn=cp1';cdn=cd1';cfn=cf1';
if ns>0
hmatsn=csn*hmat0s*csn';
end
if np>0
hmatpn=cpn*hmat0p*cpn';
end
if nd>0
hmatdn=cdn*hmat0d*cdn';
end
if nf>0
hmatfn=cfn*hmat0f*cfn';
endfor i=1:ns
    hs(i)=hmatsn(i,i);
end
for i=1:np
    hp(i)=hmatpn(i,i);
end
for i=1:nd
    hd(i)=hmatdn(i,i);
end
for i=1:nf
    hf(i)=hmatfn(i,i);
end
if ns>0 & np>0
r0fsp=r0fgto1(sbas,pbas);
rkgsp=rkggto1(sbas,pbas);
Jshsp=rkgsp(1:nprims,1:nprimp,1:nprims,1:nprimp,1)/
3;
End
 if ns>0 & nd>0
r0fsd=r0fgto1(sbas,dbas);
rkgsd=rkggto1(sbas,dbas);
Jshsd=rkgsd(1:nprims,1:nprimd,1:nprims,1:nprimd,1)/
5;
end

if ns>0 & nf>0
r0fsf=r0fgto1(sbas,fbas);
rkgsf=rkggto1(sbas,fbas);
Jshsf=rkgsf(1:nprims,1:nprimf,1:nprims,1:nprimf,1)/
7;
end

if np>0 & nd>0
r0fpd=r0fgto1(pbas,dbas);
rkgpd=rkggto1(pbas,dbas);
Jshpd = (2/15)*rkgpd(:,:,:,:,1)+
(3/35)*rkgpd(:,:,:,:,2);
end
if np>0 & nf>0
r0fpf=r0fgto1(pbas,fbas);
rkgpf=rkggto1(pbas,fbas);
Jshpf = (3/35)*rkgpf(:,:,:,:,1)+
(4/63)*rkgpf(:,:,:,:,2);
end
if nd>0 & nf>0
r0fdf=r0fgto1(dbas,fbas);
rkgdf=rkggto1(dbas,fbas);
Jshdf = (3/35)*rkgdf(:,:,:,:,1)+
(4/105)*rkgdf(:,:,:,:,2)
+ (10/231)*rkgdf(:,:,:,:,3);
end
if ns>0
r0fss=r0fgto1(sbas,sbas);
rkgss=rkggto1(sbas,sbas);
Jshs1s2=rkgss(:,:,:,:,1);
end
if np>0
r0fpp=r0fgto1(pbas,pbas);
rkgpp=rkggto1(pbas,pbas);
Jshp1p2= rkgpp(:,:,:,:,1)/3 +
2*rkgpp(:,:,:,:,2)/15;
Jshpp=(1/5)*rkgpp(:,:,:,:,2) ;
end
if nd>0
r0fdd=r0fgto1(dbas,dbas);
rkgdd=rkggto1(dbas,dbas);
Jshd1d2=rkgdd(:,:,:,:,1)/5 +
2*rkgdd(:,:,:,:,2)/35
+ 2*rkgdd(:,:,:,:,3)/35;
Jshdd = (1/14)*rkgdd(:,:,:,:,2)+
(1/14)*rkgdd(:,:,:,:,3)
end
if  nf>0
r0fff=r0fgto1(fbas,fbas);
rkgff=rkggto1(fbas,fbas);
Jshf1f2=  rkgff(:,:,:,:,1)/7 +
4*rkgff(:,:,:,:,2)/105
+ 2*rkgff(:,:,:,:,3)/77 +
100*rkgff(:,:,:,:,4)/3003;
Jshff = (2/45)*rkgff(:,:,:,:,2) +
(1/33)*rkgff(:,:,:,:,3)
+ (50/1287)*rkgff(:,:,:,:,4);
end
disp('calcul F0sp')
disp(cputime-t0)
if ns>0 & np>0
Fs0sp=zeros(nprims,nprims,np);
Fp0sp=zeros(nprimp,nprimp,ns);
  for k1=1:nprims
  for l1=1:nprims
  for k2=1:nprimp
  for l2=1:nprimp
 for j=1:np

s0sp(k1,l1,j)=Fs0sp(k1,l1,j)+cpn(j,k2)*cpn(j,l2
)
 *r0fsp(k1,l1,k2,l2);
 end
 for i=1:ns
Fp0sp(k2,l2,i)=Fp0sp(k2,l2,i)+csn(i,k1)*csn(i,l
1)
 *r0fsp(k1,l1,k2,l2);
 end;  end;  end;  end; end;
disp('calcul Gksp')
disp(cputime-t0)
Js_sp=zeros(nprims,nprims,np);
Jp_sp=zeros(nprimp,nprimp,ns);
  for k1=1:nprims
  for k2=1:nprims
  for l1=1:nprimp
  for l2=1:nprimp
for j=1:np
Js_sp(k1,k2,j)=Js_sp(k1,k2,j)+cpn(j,l1)
*cpn(j,l2)*Jshsp(k1,l1,k2,l2);
end
for i=1:ns
Jp_sp(l1,l2,i)=Jp_sp(l1,l2,i)+csn(i,k1)
*csn(i,k2)*Jshsp(k1,l1,k2,l2);
end; end; end; end; end; end
disp('calcul F0sd')
disp(cputime-t0)
if ns>0 & nd>0
```

```
Fs0sd=zeros(nprims,nprims,nd);
Fd0sd=zeros(nprimd,nprimd,ns);
  for k1=1:nprims
  for k2=1:nprimd
  for l1=1:nprims
  for l2=1:nprimd
for j=1:nd
Fs0sd(k1,l1,j)=Fs0sd(k1,l1,j)+cdn(j,k2)*cdn(j,l
2)
*r0fsd(k1,l1,k2,l2);
end
for i=1:ns
Fd0sd(k2,l2,i)=Fd0sd(k2,l2,i)+csn(i,k1)*csn(i,l
1)
*r0fsd(k1,l1,k2,l2);
end;  end;  end;  end;  end;
disp('calcul Gksd')
disp(cputime-t0)
Js_sd=zeros(nprims,nprims,nd);
Jd_sd=zeros(nprimd,nprimd,ns);
   for k1=1:nprims
  for k2=1:nprims
  for l1=1:nprimd
  for l2=1:nprimd
for j=1:nd
Js_sd(k1,k2,j)=Js_sd(k1,k2,j)+cdn(j,l1)*
cdn(j,l2)*Jshsd(k1,l1,k2,l2);
end
for i=1:ns
Jd_sd(l1,l2,i)=Jd_sd(l1,l2,i)+csn(i,k1)
*csn(i,k2)*Jshsd(k1,l1,k2,l2);
end;  end;  end;  end;  end; end
disp('calcul F0sf')
disp(cputime-t0)
if ns>0 & nf>0
Fs0sf=zeros(nprims,nprims,nf);
Ff0sf=zeros(nprimf,nprimf,ns);
  for k1=1:nprims
  for k2=1:nprimf
  for l1=1:nprims
  for l2=1:nprimf
 for j=1:nf
 Fs0sf(k1,l1,j)=Fs0sf(k1,l1,j)+cfn(j,k2)
*cfn(j,l2)*r0fsf(k1,l1,k2,l2);
 end
for i=1:ns
 Ff0sf(k2,l2,i)=Ff0sf(k2,l2,i)+csn(i,k1)
*csn(i,l1)*r0fsf(k1,l1,k2,l2);
 end;  end;  end;  end;  end
disp('calcul Gksf')
disp(cputime-t0)
Js_sf=zeros(nprims,nprims,nf);
Jf_sf=zeros(nprimf,nprimf,ns);
  for k1=1:nprims
  for k2=1:nprims
  for l1=1:nprimf
  for l2=1:nprimf
for j=1:nf
 Js_sf(k1,k2,j)=Js_sf(k1,k2,j)+cfn(j,l1)
*cfn(j,l2)*Jshsf(k1,l1,k2,l2);
end
for i=1:ns
 Jf_sf(l1,l2,i)=Jf_sf(l1,l2,i)+csn(i,k1)
*csn(i,k2)*Jshsf(k1,l1,k2,l2);
End;   end ;  end;  end;  end; end
disp('calcul F0pd')
disp(cputime-t0)
if np>0 & nd>0
Fp0pd=zeros(nprimp,nprimp,nd);
Fd0pd=zeros(nprimd,nprimd,np);
  for k1=1:nprimp
  for k2=1:nprimd
  for l1=1:nprimp
  for l2=1:nprimd
for j=1:nd
Fp0pd(k1,l1,j)=Fp0pd(k1,l1,j)+cdn(j,k2)*
cdn(j,l2) *r0fpd(k1,l1,k2,l2);
end
 for i=1:np
Fd0pd(k2,l2,i)=Fd0pd(k2,l2,i)+cpn(i,k1)*cpn(i,l
1) *r0fpd(k1,l1,k2,l2);
 end;  end;  end;  end;  end
disp('calcul Gkpd')
disp(cputime-t0)
Jp_pd=zeros(nprimp,nprimp,nd);
Jd_pd=zeros(nprimd,nprimd,np);
  for k1=1:nprimp
  for k2=1:nprimp
  for l1=1:nprimd
 for l2=1:nprimd
 for j=1:nd
Jp_pd(k1,k2,j)=Jp_pd(k1,k2,j)+cdn(j,l1)*cdn(j,l
2) *Jshpd(k1,l1,k2,l2);
 end
 for i=1:np
J_pd(l1,l2,i)=Jd_pd(l1,l2,i)+cpn(i,k1)*cpn(i,k2
) *Jshpd(k1,l1,k2,l2);
 end;  end;  end;  end;  end; end
disp('calcul F0pf')
disp(cputime-t0)
if np>0 & nf>0
 Fp0pf=zeros(nprimp,nprimp,nf);
 Ff0pf=zeros(nprimf,nprimf,np);
  for k1=1:nprimp
  for k2=1:nprimf
  for l1=1:nprimp
  for l2=1:nprimf
 for j=1:nf
Fp0pf(k1,l1,j)=Fp0pf(k1,l1,j)+cfn(j,k2)*
cfn(j,l2)*r0fpf(k1,l1,k2,l2);
 end
for i=1:np
Ff0pf(k2,l2,i)=Ff0pf(k2,l2,i)+cpn(i,k1)*cpn(i,l
1)
*r0fpf(k1,l1,k2,l2);
end;  end;  end;  end;  end
disp('calcul Gkpf')
disp(cputime-t0)
Jp_pf=zeros(nprimp,nprimp,nf);
Jf_pf=zeros(nprimf,nprimf,np);
  for k1=1:nprimp
  for k2=1:nprimp
  for l1=1:nprimf
  for l2=1:nprimf
for j=1:nf
  Jp_pf(k1,k2,j)=Jp_pf(k1,k2,j)+cfn(j,l1)
*cfn(j,l2)  *Jshpf(k1,l1,k2,l2);
end
for i=1:np
  Jf_pf(l1,l2,i)=Jf_pf(l1,l2,i)+cpn(i,k1)
*cpn(i,k2)  *Jshpf(k1,l1,k2,l2);
end;  end;  end;  end;  end; end
disp('calcul F0df')
disp(cputime-t0)
if nd>0 & nf>0
Fd0df=zeros(nprimd,nprimd,nf);
Ff0df=zeros(nprimf,nprimf,nd);
  for k1=1:nprimd
  for k2=1:nprimf
  for l1=1:nprimd
  for l2=1:nprimf
for j=1:nf
Fd0df(k1,l1,j)=Fd0df(k1,l1,j)+cfn(j,k2)
*cfn(j,l2)*r0fdf(k1,l1,k2,l2);
end
  for i=1:nd
  Ff0df(k2,l2,i)=Ff0df(k2,l2,i)+cdn(i,k1)
*cdn(i,l1)*r0fdf(k1,l1,k2,l2);
```

```
end;  end;  end;  end;  end
disp('calcul Gkdf') disp(cputime-t0)
Jd_df=zeros(nprimd,nprimd,nf);
Jf_df=zeros(nprimf,nprimf,nd);
  for k1=1:nprimd
  for k2=1:nprimd
  for l1=1:nprimf
  for l2=1:nprimf
for j=1:nf
  Jd_df(k1,k2,j)=Jd_df(k1,k2,j)+cfn(j,l1)
*cfn(j,l2)*Jshdf(k1,l1,k2,l2);
end
for i=1:nd
  Jf_df(l1,l2,i)=Jf_df(l1,l2,i)+cdn(i,k1)
*cdn(i,k2)*Jshdf(k1,l1,k2,l2);
end;  end;  end;  end;  end; end
disp('calcul F0s1s2')
disp(cputime-t0)
if ns>0
Fs0s1s2=zeros(nprims,nprims,ns);
  for k1=1:nprims
  for k2=1:nprims
  for l1=1:nprims
  for l2=1:nprims
for j=1:ns
Fs0s1s2(k1,l1,j)=Fs0s1s2(k1,l1,j)+csn(j,k2)
 *csn(j,l2)*r0fss(k1,l1,k2,l2);
end;  end;  end;  end;  end
disp('calcul Gks1s2')
disp(cputime-t0)
Js_s1s2=zeros(nprims,nprims,ns);
  for k1=1:nprims
  for k2=1:nprims
  for l1=1:nprims
  for l2=1:nprims
for j=1:ns
  Js_s1s2(k1,k2,j)=Js_s1s2(k1,k2,j)+csn(j,l1)
  *csn(j,l2)*Jshs1s2(k1,l1,k2,l2);
end; end;  end;  end;  end
disp('calcul F0ss')
disp(cputime-t0)
Fs0ss=zeros(nprims,nprims,ns);
  for k1=1:nprims
  for k2=1:nprims
  for l1=1:nprims
  for l2=1:nprims
for i=1:ns
Fs0ss(k1,l1,i)=Fs0ss(k1,l1,i)+csn(i,k2)*csn(i,l
2) *r0fss(k1,l1,k2,l2);
end; end;  end;  end;  end; end
disp('calcul F0p1p2')
disp(cputime-t0)
if np>0
Fp0p1p2=zeros(nprimp,nprimp,np);
  for k1=1:nprimp
  for k2=1:nprimp
  for l1=1:nprimp
  for l2=1:nprimp
for j=1:np
  Fp0p1p2(k1,l1,j)= Fp0p1p2(k1,l1,j)+cpn(j,k2)
  *cpn(j,l2)*r0fpp(k1,l1,k2,l2);
end; end;  end;  end;  end
disp('calcul Gkp1p2')
disp(cputime-t0)
Jp_p1p2=zeros(nprimp,nprimp,np);
  for k1=1:nprimp
  for k2=1:nprimp
  for l1=1:nprimp
  for l2=1:nprimp
for j=1:np
Jp_p1p2(k1,k2,j)=Jp_p1p2(k1,k2,j)+cpn(j,l1)*
  cpn(j,l2)*Jshp1p2(k1,l1,k2,l2);
end; end;  end;  end;  end
 disp('calcul F0pp')
disp(cputime-t0)
Jp_pp=zeros(nprimp,nprimp,np);
  for k1=1:nprimp
  for k2=1:nprimp
  for l1=1:nprimp
  for l2=1:nprimp
for i=1:np
  Jp_pp(k1,k2,i)=Jp_pp(k1,k2,i)+cpn(i,l1)*
  cpn(i,l2)*Jshpp(k1,l1,k2,l2);
end; end;  end;  end;  end; end
disp('calcul F0d1d2')
disp(cputime-t0)
if nd>0
Fd0d1d2=zeros(nprimd,nprimd,nd);
  for k1=1:nprimd
  for k2=1:nprimd
  for l1=1:nprimd
  for l2=1:nprimd
 for j=1:nd
 Fd0d1d2(k1,l1,j)=Fd0d1d2(k1,l1,j)+cdn(j,k2)
 *cdn(j,l2)*r0fdd(k1,l1,k2,l2);
 end; end;  end;  end;  end
disp('calcul Gkd1d2')
disp(cputime-t0)
Jd_d1d2=zeros(nprimd,nprimd,nd);
  for k1=1:nprimd
  for k2=1:nprimd
  for l1=1:nprimd
  for l2=1:nprimd
for j=1:nd
 Jd_d1d2(k1,k2,j)=Jd_d1d2(k1,k2,j)+cdn(j,l1)
 *cdn(j,l2)*Jshd1d2(k1,l1,k2,l2);
end; end;  end;  end;  end
disp('calcul F0dd')
disp(cputime-t0)
Fd0dd=zeros(nprimd,nprimd,nd);
  for k1=1:nprimd
  for k2=1:nprimd
  for l1=1:nprimd
  for l2=1:nprimd
 for i=1:nd
  Fd0dd(k1,l1,i)=Fd0dd(k1,l1,i)+cdn(i,k2)
  *cdn(i,l2)*r0fdd(k1,l1,k2,l2);
end; end;  end;  end;  end
disp('calcul Gkdd')
disp(cputime-t0)
Jd_dd=zeros(nprimd,nprimd,nd);
  for k1=1:nprimd
  for k2=1:nprimd
  for l1=1:nprimd
  for l2=1:nprimd
 for i=1:nd
 Jd_dd(k1,k2,i)=Jd_dd(k1,k2,i)+cdn(i,l1)
 *cdn(i,l2)*Jshdd(k1,l1,k2,l2);
end; end;  end;  end;  end; end
disp('calcul F0f1f2')
disp(cputime-t0)
if  nf>0
Ff0f1f2=zeros(nprimf,nprimf,nf);
  for k1=1:nprimf
  for k2=1:nprimf
  for l1=1:nprimf
  for l2=1:nprimf
for j=1:nf
  Ff0f1f2(k1,l1,j)=Ff0f1f2(k1,l1,j)+cfn(j,k2)
  *cfn(j,l2)*r0fff(k1,l1,k2,l2);
end; end;  end;  end;  end
disp('calcul Gkf1f2'); disp(cputime-t0)
Jf_f1f2=zeros(nprimf,nprimf,nf);
  for k1=1:nprimf
  for k2=1:nprimf
  for l1=1:nprimf
  for l2=1:nprimf
for j=1:nf
  Jf_f1f2(k1,k2,j)=Jf_f1f2(k1,k2,j)+cfn(j,l1)
  *cfn(j,l2)*Jshf1f2(k1,l1,k2,l2);
end; end;  end;  end;  end
```

```
disp('calcul F0ff')
disp(cputime-t0)
Ff0ff=zeros(nprimf,nprimf,nf);
for i=1:nf
  for k1=1:nprimf
  for k2=1:nprimf
  for l1=1:nprimf
  for l2=1:nprimf
  Ff0ff(k1,l1,i)=Ff0ff(k1,l1,i)+cfn(i,k2)
  *cfn(i,l2)*rkgff(k1,l1,k2,l2);
end; end;  end;  end;  end
   disp('calcul Gkff')
disp(cputime-t0)
Jf_ff=zeros(nprimf,nprimf,nf);
  for k1=1:nprimf
  for k2=1:nprimf
  for l1=1:nprimf
  for l2=1:nprimf
for i=1:nf
   Jf_ff(k1,k2,i)=Jf_ff(k1,k2,i)+cfn(i,l1)
   *cfn(i,l2)*Jshff(k1,l1,k2,l2);
end; end;  end;  end;  end; end
disp('calcul S')
disp(cputime-t0)
 for i=1:nsocc
    if ps(i)<1.0
        Ss(i)=ps(i)/2;
    else
        Ss(i)=1-(ps(i))/2;
    end; end
for i=1:npocc
    if pp(i)<3.0
        Sp(i)=pp(i)/2;
    else
        Sp(i)=3-(pp(i))/2 ;
    end
end
for i=1:ndocc
    if pd(i)<5.0
        Sd(i)=pd(i)/2;
    else
        Sd(i)=5-(pd(i))/2 ;
    end
end
for i=1:nfocc
    if pf(i)<7.0
        Sf(i)=pf(i)/2;
    else
        Sf(i)=7-(pf(i))/2 ;
    end; end
for i=nsocc+1:ns
ps(i)=0; Ss(i)=0;
end
for i=npocc+1:np
pp(i)=0; Sp(i)=0;
end
for i=ndocc+1:nd
pd(i)=0; Sd(i)=0;
end
for i=nfocc+1:nf
pf(i)=0; Sf(i)=0;
end
disp('calcul E')
disp(cputime-t0)
ps pp pd
Ss Sp Sd
fmatsn=zeros(ns,ns);
fmatpn=zeros(np,np);
fmatdn=zeros(nd,nd);
fmatfn=zeros(nf,nf);
fmatsnl=zeros(ns,ns);
fmatpnl=zeros(np,np);
fmatdnl=zeros(nd,nd);
fmatfnl=zeros(nf,nf);
Es=0;
for i=1:nsocc
add1=csn(i,:)*Fs0ss(:,:,i)*csn(i,:)';
 fmatsn(i,i)=fmatsn(i,i)+(ps(i)-1)*add1;
 Es=Es+ps(i)*hs(i)+ps(i)*fmatsn(i,i);
end
h1s=hmatsn(1,1);
h2s=hmatsn(2,2);
F01s=csn(1,:)*Fs0ss(:,:,1)*csn(1,:)';;
F02s=csn(2,:)*Fs0ss(:,:,2)*csn(2,:)';;
Ep=0;
for i=1:npocc
 add1=cpn(i,:)*Fp0pp(:,:,i)*cpn(i,:)';
 add2=cpn(i,:)*Jp_pp(:,:,i)*cpn(i,:)';
fmatpn(i,i)=fmatpn(i,i)+(pp(i)-1)*add1-(1/16)*
(10*pp(i)-19)*add2;
fmatpnl(i,i)=fmatpnl(i,i)-
(3/16)*(4*Sp(i)+1)*add2;
 Ep=Ep+pp(i)*hp(i)+pp(i)*fmatpn(i,i)+Sp(i)
 *fmatpnl(i,i);
end
h2p=hmatpn(1,1);
F02p=add1(1,1);
J2p=add2(1,1);
Ed=0;
for i=1:ndocc
 add1=cdn(i,:)*Fd0dd(:,:,i)*cdn(i,:)';
 add2=cdn(i,:)*Jd_dd(:,:,i)*cdn(i,:)';
 fmatdn(i,i)=fmatdn(i,i)+2*(1/2)*(pd(i)-1)*
 add1-2*(1/24)* (7*pd(i)-22)*add2;
 fmatdnl(i,i)=fmatdnl(i,i)-
2*(5/6)*(Sd(i)+1)*add2;
 Ed=Ed+pd(i)*hd(i)+pd(i)*fmatdn(i,i)+Sd(i)
 *fmatdnl(i,i);;
end
Ef=0;
for i=1:nfocc
 add1=cfn(i,:)*Ff0ff(:,:,i)*cfn(i,:)';
 add2=cfn(i,:)*Jf_ff(:,:,i)*cfn(i,:)';
 fmatfn(i,i)=fmatfn(i,i)+2*(1/2)*(pf(i)-1)
 *add1-2*(1/32)*(9*pf(i)-30)*add2;
 fmatfnl(i,i)=fmatfnl(i,i)-
2*(7/8)*(Sf(i)+1)*add2;
 Ef=Ef+pf(i)*hf(i)+pf(i)*fmatfn(i,i)+Sf(i)
 *fmatfnl(i,i);;
end
Esp=0;
if nprims>0
for i=1:npocc
 add1=csn*Fs0sp(:,:,i)*csn';
 add2=csn*Js_sp(:,:,i)*csn';
 fmatsn=fmatsn+pp(i)*add1-(1/2)*pp(i)*add2;
 fmatsnl=fmatsnl-2*Sp(i)*add2;
for j=1:ns; Esp=Esp+ ps(j)*(pp(i)*add1(j,j)-
(1/2)
    *pp(i)*add2(j,j)); end
end; end
F01s2p=add1(1,1);
J1s2p=add2(1,1);
F02s2p=add1(2,2);
J2s2p=add2(2,2);
if nprimp>0
for i=1:nsocc
 add1=cpn*Fp0sp(:,:,i)*cpn';
 add2=cpn*Jp_sp(:,:,i)*cpn';
 fmatpn=fmatpn+ps(i)*add1-(1/2)*ps(i)*add2;
 fmatpnl=fmatpnl-2*Ss(i)*add2;
 for j=1:np; Esp=Esp+ pp(j)*(ps(i)*add1(j,j)-
(1/2)
     *ps(i)*add2(j,j)); end
end; end
if nprims>0
for i=1:ndocc
 add1=csn*Fs0sd(:,:,i)*csn';
 add2=csn*Js_sd(:,:,i)*csn';
 fmatsn=fmatsn+pd(i)*add1-(1/2)*pd(i)*add2;
 fmatsnl=fmatsnl-2*Sd(i)*add2;
end; end
```

```
if nprimd>0
for i=1:nsocc
 add1=cdn*Fd0sd(:,:,i)*cdn';
 add2=cdn*Jd_sd(:,:,i)*cdn';
 fmatdn=fmatdn+ps(i)*add1-(1/2)*ps(i)*add2;
 fmatdn1=fmatdn1-2*Ss(i)*add2;
end; end
if nprims>0
for i=1:nfocc
 add1=csn*Fs0sf(:,:,i)*csn';
 add2=csn*Js_sf(:,:,i)*csn';
 fmatsn=fmatsn+pf(i)*add1-(1/2)*pf(i)*add2;
 fmatsn1=fmatsn1-2*Sf(i)*add2;
 end; end
if nprimf>0
for i=1:nsocc
 add1=cfn*Ff0sf(:,:,i)*cfn';
 add2=cfn*Jf_sf(:,:,i)*cfn';
 fmatfn=fmatfn+ps(i)*add1-(1/2)*ps(i)*add2;
 fmatfn1=fmatfn1-2*Ss(i)*add2;
end; end
if nprimp>0
for i=1:ndocc
 add1=cpn*Fp0pd(:,:,i)*cpn';
 add2=cpn*Jp_pd(:,:,i)*cpn';
 fmatpn=fmatpn+pd(i)*add1-(1/2)*pd(i)*add2;
 fmatpn1=fmatpn1-2*Sd(i)*add2;
end; end
if nprimd>0
for i=1:npocc
 add1=cdn*Fd0pd(:,:,i)*cdn';
 add2=cdn*Jd_pd(:,:,i)*cdn';
 fmatdn=fmatdn+pp(i)*add1-(1/2)*pp(i)*add2;
 fmatdn1=fmatdn1-2*Sp(i)*add2;
end; end
if nprimp>0
for i=1:nfocc
 add1=cpn*Fp0pf(:,:,i)*cpn';
 add2=cpn*Jp_pf(:,:,i)*cpn';
 fmatpn=fmatpn+pf(i)*add1-(1/2)*pf(i)*add2;
 fmatpn1=fmatpn1-2*Sf(i)*add2;
end; end
if nprimf>0
for i=1:npocc
 add1=cfn*Ff0pf(:,:,i)*cfn';
 add2=cfn*Jf_pf(:,:,i)*cfn';
 fmatfn=fmatfn+pp(i)*add1-(1/2)*pp(i)*add2;
 fmatfn1=fmatfn1-2*Sp(i)*add2;
end; end
if nprimd>0
for i=1:nfocc
 add1=cdn*Fd0df(:,:,i)*cdn';
 add2=cdn*Jd_df(:,:,i)*cdn';
 fmatdn=fmatdn+pf(i)*add1-(1/2)*pf(i)*add2;
 fmatdn1=fmatdn1-2*Sf(i)*add2;
end; end
if nprimf>0
for i=1:ndocc
 add1=cfn*Ff0df(:,:,i)*cfn';
 add2=cfn*Jf_df(:,:,i)*cfn';
 fmatfn=fmatfn+pd(i)*add1-(1/2)*pd(i)*add2;
 fmatfn1=fmatfn1-2*Sd(i)*add2;
end; end
Es1s2=0;
if nprims>0
for i=1:nsocc
 add1=csn*Fs0s1s2(:,:,i)*csn';
 add2=csn*Js_s1s2(:,:,i)*csn';
 add1(i,i)=0; add2(i,i)=0;
 fmatsn=fmatsn+ps(i)*add1-(1/2)*ps(i)*add2;
 fmatsn1=fmatsn1-2*Ss(i)*add2;
 for j=1:ns; Es1s2=Es1s2+
ps(j)*(ps(i)*add1(j,j)
     -(1/2)*ps(i)*add2(j,j)); end
end; end
F01s2s=add1(1,1);
J1s2s=add2(1,1);
 Ep1p2=0;
if nprimp>0
for i=1:npocc
 add1=cpn*Fp0p1p2(:,:,i)*cpn';
 add2=cpn*Jp_p1p2(:,:,i)*cpn';
 add1(i,i)=0; add2(i,i)=0;
 fmatpn=fmatpn+pp(i)*add1-(1/2)*pp(i)*add2;
 fmatpn1=fmatpn1-2*Sp(i)*add2;
 for j=1:np; Ep1p2=Ep1p2+  pp(j)*(pp(i)*
     add1(j,j)-(1/2)*pp(i)*add2(j,j)); end
end; end
if nprimd>0
for i=1:ndocc
 add1=cdn*Fd0d1d2(:,:,i)*cdn';
 add2=cdn*Jd_d1d2(:,:,i)*cdn';
 add1(i,i)=0; add2(i,i)=0;
 fmatdn=fmatdn+pd(i)*add1-(1/2)*pd(i)*add2;
 fmatdn1=fmatdn1-2*Sd(i)*add2;
end; end
 if nprimf>0
for i=1:nfocc
 add1=cfn*Ff0f1f2(:,:,i)*cfn';
 add2=cfn*Jf_f1f2(:,:,i)*cfn';
 add1(i,i)=0; add2(i,i)=0;
 fmatfn=fmatfn+pf(i)*add1-(1/2)*pf(i)*add2;
 fmatfn1=fmatfn1-2*Sf(i)*add2;
end; end
if ns>0
 fmatsn=hmatsn+fmatsn;
end
if np>0
 fmatpn=hmatpn+fmatpn;
end
if nd>0
fmatdn=hmatdn+fmatdn;
end
if nf>0
fmatfn=hmatfn+fmatfn;
end
Etot=0;
for i=1:nsocc
 Etot=Etot+0.5*ps(i)*(hmatsn(i,i)+fmatsn(i,i))
 +0.5*Ss(i)*fmatsn1(i,i);
end
for i=1:npocc
 Etot=Etot+0.5*pp(i)*(hmatpn(i,i)+fmatpn(i,i))
 +0.5*Sp(i)*fmatpn1(i,i);
end
for i=1:ndocc
 Etot=Etot+0.5*pd(i)*(hmatdn(i,i)+fmatdn(i,i))
 +0.5*Sd(i)*fmatdn1(i,i);
end
for i=1:nfocc
 Etot=Etot+0.5*pf(i)*(hmatfn(i,i)+fmatfn(i,i))
 +0.5*Sf(i)*fmatfn1(i,i);;
end
Etot
disp('final')
disp(cputime-t0)
```

References

[1] Jensen, F. *Introduction to Quantum Chemistry*, Wiley, New York, **2002**.

[2] (a) Hehre, W.J.; Stewart, R.F.; Pople, J.A. *J. Chem. Phys.* **1969**, *51*, 2657-64. (b) Hehre, W. J.; Ditchfiel, R.; Pople, J. A. *J. Chem. Phys.* **1972**, *56*, 2257-2266.

[3] Gordon, M. S.; Binkley, J.S.; Pople, J.A.; Pietro, W. J.; Hehre, W. J. *J. Am. Chem. Soc.* **1982**, *104*, 2797-803.

[4] (a) Schaefer, A.; Horn, H.; Ahlrichs, R. *J. Chem. Phys.* **1992**, *97*, 2571-2577. (b) Schaefer, A.; Huber, C.; Ahlrichs, R. *J. Chem. Phys.* **1994**, *100*, 5829-5835; (c) Weigend, F.; Ahlrichs, R. *Phys. Chem. Chem. Phys*. **2005**, *7*, 3297-3305

[5] (a) Dunning Jr., T. H. *J. Chem. Phys.* **1989**, *90*, 1007-1023 (b) Woon, D.E.; Dunning Jr., T.H. *J. Chem. Phys.* **1993**, *98*, 1358-1371.

[6] (a) Widmark, P. O.; Malmqvist, P. A.; Roos, B. O. *Theor. Chim. Acta* **1990**, *77*, 291-306. (b) Roos, B.O.; Lindh, R.; Malmqvist, P. A.; Veryazov, V.; Widmark, P. O. *J. Phys. Chem. A* **2005**, *108*(15), 2851-2858. (c) Roos, B.O.; Lindh, R.; Malmqvist, P. A.; Veryazov, V.; Widmark, P. O. *J. Phys. Chem. A* **2005**, *109*, 6575-6579.

[7] (a) Hay, P. J.; Wadt, W. R. *J. Chem. Phys.* **1985**, *82*, 270-283. (b) Stevens, W. J.; Krauss, M.; Basch, H.; Jasien, P. G. *Can. J. Chem.* **1992**, *70*, 612-630.

[8] Ferbinteanu, M.; Cimpoesu, F.; Tanase, S. *Structure and Bonding* **2015**, *163*, 185-229

[9] Ramanantoanina, H.; Urland, W.; Herden, B.; Cimpoesu, F.; Daul, C.. *Phys. Chem. Chem. Phys.* **2015**, *17*, 9116-9125.

[10] Kresse, G.; Furthmüller, J. Efficient iterative schemes for ab initio total-energy calculations using a plane-wave basis set. *Phys. Rev. B: Condens. Matter Mater. Phys*. **1996**, *54*, 11169-11186.

[11] NIST: Atomic Spectra Database - Energy Levels Form, https://physics.nist.gov/PhysRefData/ASD/levels_form.html

[12] Ferbinteanu, M.; Stroppa, A.; Scarrozza, M.; Humelnicu, I.; Maftei, D.; Frecus, B.; Cimpoesu, F. Inorg. Chem., 2017, 56 (16), 9474–9485, DOI: 10.1021/acs.inorgchem.7b00587

[13] Costes, J.-P.; Dahan, F.; Dupuis, A. and Laurent, J.-P. *New J. Chem.*, **1998**, *22*, 1525-1529.

[14] Noodleman, L.; Peng, C.Y.; Case, D.A.; Mouesca, J. M. *Coord. Chem. Rev.* **1995**, *144*, 199-244., Ruiz, E. *Struct. Bonding* **2004**, *113*, 71-102.

[15] Cremades, E.; Gómez-Coca, S.; Aravena, D.; Alvarez, S.; Ruiz, E. *J. Am. Chem. Soc.* **2012**, *134*, 10532-10542

[16] Schmidt, M. W.; Baldridge, K. K.; Boatz, J. A.; Elbert, S. T.; Gordon, M. S.; Jensen, J. H.; Koseki, S.; Matsunaga, N.; Nguyen, K. A.; Su, S. J.; Windus, T. L.; Dupuis, M.; Montgomery, J. A. General Atomic and Molecular Electronic Structure System. *J. Comput. Chem.* **1993**, *14*, 1347-1363.

[17] Costes, J.-P.; Dahan, F.; and Wernsdorfer,W. *Inorg. Chem.,* **2006**, 45, 5-7

[18] Koch, W.; Holthausen, M. C. *A Chemist's Guide to Density Functional Theory*, Wiley-VCH: Berlin, **2001**.

[19] (a) Onishi, T.; Takano, Y.; Kitagawa, Y.; Kawakami, T.; Yoshioka, Y.; Yamaguchi, K. *Polyhedron* **2001**, *20*, 1177. (b) Nagao, H.; Nishino, M.; Shigeta, Y.; Soda, T.; Kitagawa, Y.; Onishi, T.; Yoshioka, Y.; Yamaguchi, K. *Coord. Chem. Rev.* **2000**, *198*, 265-295.

[20] Dudarev, S. L.; Botton, G. A.; Savrasov, S. Y.; Humphreys, C. J.; Sutton, A. P. *Phys. Rev. B* **1998**, *57*, 1505-1509.

[21] Newman, D. J.; Ng, B. K. C. *Crystal Field Handbook*, Cambridge University Press, Cambridge, **2000**.

[22] R. D. Cowan, The Theory of Atomic Structure and Spectra, University of California Press, Berkeley, **1981**.

[23] Boys, S. F. Electronic Wave Functions. 1. A General Method of Calculation for the Stationary States of Any Molecular System. *Proc. Roy. Soc. London A: Mat. Sci.* **1950**, *200*, 542.

[24] Nagy, B. & Jensen, F. *Basis Sets in Quantum Chemistry, in Reviews in Computational Chemistry*, *50,* 93-149, John Willey & Sons, New Jersey, **2018**.

[25] Abramowitz, M. & Stegun, I. A. *Handbook of mathematical functions, Tenth Printing*, 253-294, Washington, **1972**.

[26] Slater, J. Analytic atomic wave functions. *Phys. Rev.* **1932**, *42*, 33-43.

[27] A notable suite based on the Slater-Type Orbitals is the ADF code (Amsterdam Density Functional): ADF Van Lenthe, E. and Baerends, E.J. Optimized Slater-Type Basis Sets for the Elements 1–118. *J. Comput. Chem*. **2003**, *24*, 1142–1156.

[28] (a) Daul, C. A. E. Xatom, [http://www.chem.unifr.ch/cd/download/files/Xatom_lite.zip].
(b) de Castro, E. V. R., Jorge, F. E. *J. Chem. Phys*. **1998**, *108*, 5225-5229. (c) Borel, A.; Helm, L.; Daul, C. A. E. *Chem. Phys. Lett.* **2004**, *383*, 584-591. (d) Weber, V.; Daul, C.; Baltensperger, R.; *Comput. Phys. Commun*. **2004**, *163*(3), 133-142.

[29] National Institute of Standards and Technology (NIST). Atomic Spectra Database Levels Data, https://physics.nist.gov/PhysRefData/ASD/levels_form.html

[30] Putz, M. V.; Cimpoesu, F.; Ferbinteanu, M. *Structural Chemistry, Principles, Methods, and Case Studies*, Springer, Cham, **2018**, 107-220.

[31] Gao, Y.; Viciano-Chumillas, M.; Toader, A. M.; Teat, S. J.; Ferbinteanu M.; Tanase S. *Inorg. Chem. Front*., **2018**, *5*, 1967-1977.

[32]. Weber, V.; Daul, C.; Baltensperger, R. Radial numerical integrations based on the sinc function. *Comput. Phys. Commun*. **2004**, *163(3)*, 133-142. https://doi.org/10.1016/j.cpc.2004.08.008

[33] Amabilino, D.B.; Veciana, J. Magnetism, Molecules to Materials II; Miller, J.S., Drillon, M., Eds.;Wiley-VCH: Weinheim, Germany, 2001; Volume II, pp. 1–60.

[34] Abe, M. Diradicals. Chem. Rev. **2013**, 113, 7011–7088.